

## Extended hadron and two-hadron operators of definite momentum for spectrum calculations in lattice QCD

C. Morningstar,<sup>1</sup> J. Bulava,<sup>2,3</sup> B. Fahy,<sup>1</sup> J. Foley,<sup>4</sup> Y. C. Jhang,<sup>1</sup> K. J. Juge,<sup>5</sup> D. Lenkner,<sup>1</sup> and C. H. Wong<sup>6</sup><sup>1</sup>*Department of Physics, Carnegie Mellon University, Pittsburgh, Pennsylvania 15213, USA*<sup>2</sup>*School of Mathematics, Trinity College, Dublin 2, Ireland*<sup>3</sup>*Physics Department, CERN, CH-1211 Geneva 23, Switzerland*<sup>4</sup>*Department of Physics and Astronomy, University of Utah, Salt Lake City, Utah 84112, USA*<sup>5</sup>*Department of Physics, University of the Pacific, Stockton, California 95211, USA*<sup>6</sup>*Department of Physics, University of California at San Diego, La Jolla, California 92093, USA*

(Received 27 March 2013; published 23 July 2013)

Multihadron operators are crucial for reliably extracting the masses of excited states lying above multihadron thresholds in lattice QCD Monte Carlo calculations. The construction of multihadron operators with significant coupling to the lowest-lying multihadron states of interest involves combining single hadron operators of various momenta. The design and implementation of large sets of spatially-extended single-hadron operators of definite momentum and their combinations into two-hadron operators are described. The single hadron operators are all assemblages of gauge-covariantly-displaced, smeared quark fields. Group-theoretical projections onto the irreducible representations of the symmetry group of a cubic spatial lattice are used in all isospin channels. Tests of these operators on  $24^3 \times 128$  and  $32^3 \times 256$  anisotropic lattices using a stochastic method of treating the low-lying modes of quark propagation which exploits Laplacian Heaviside quark-field smearing are presented. The method provides reliable estimates of all needed correlations, even those that are particularly difficult to compute, such as  $\eta\eta \rightarrow \eta\eta$  in the scalar channel, which involves the subtraction of a large vacuum expectation value. A new glueball operator is introduced, and the evaluation of the mixing of this glueball operator with a quark-antiquark operator,  $\pi\pi$ , and  $\eta\eta$  operators is shown to be feasible.

DOI: [10.1103/PhysRevD.88.014511](https://doi.org/10.1103/PhysRevD.88.014511)

PACS numbers: 12.38.Gc, 11.15.Ha, 12.39.Mk

### I. INTRODUCTION

Markov-chain Monte Carlo estimates of quantum chromodynamics (QCD) path integrals defined on a space-time lattice are a promising means of calculating the mass spectrum of excited-state hadron resonances. Because of the way in which stationary-state energies are extracted from the temporal correlations of suitable quantum field operators in such calculations, the energy of a particular state of interest can only be determined after contributions from all lower-lying and nearby states in the same symmetry channel are carefully considered. Multihadron states populate the spectrum below most of the resonances of interest. To reliably determine the energies of such states, the use of appropriate multihadron operators is crucial. Multihadron operators with significant coupling to the low-lying states of interest can be obtained by combining single-hadron operators of various momenta. The construction and testing of single-hadron operators of definite momentum and their combinations into two-hadron operators are the subject of this work.

Our approach to constructing single baryon operators of zero momentum was previously described in Ref. [1]. A slightly different method was reported in Ref. [2]. Our first study of the nucleon and  $\Delta$  excitations in the quenched approximation was presented in Ref. [3], and nucleon results for two flavors of dynamical quarks appeared in Ref. [4]. A survey of excited-state energies in small volume

for the isovector mesons and kaons using  $N_f = 2 + 1$  dynamical quarks was given in Ref. [5], along with results for the  $\Lambda$ ,  $\Sigma$ ,  $\Xi$  baryons. To extend our efforts into larger volumes and towards  $u$ ,  $d$  quark masses yielding lighter pions, the issue of multihadron states was addressed in Ref. [6]. A new stochastic method of treating the low-lying modes of quark propagation which exploits Laplacian Heaviside (LapH) quark-field smearing was presented in that work, although the method was briefly introduced with preliminary testing in Refs. [5,7,8]. Other recent progress in calculating excited-state energies in lattice QCD can be found in Refs. [9–24].

In this work, the approach of Ref. [1] is extended to meson operators of zero momentum and to both meson and baryon operators having definite nonzero momentum. A new glueball operator is also introduced and tested. To simplify our spectrum calculations as much as possible and to increase the statistical precision of our results, we make use of single-hadron operators that transform irreducibly under all symmetries of a three-dimensional cubic lattice with periodic boundary conditions. Our method of constructing such operators is described in detail in this paper. Spectrum results obtained using these operators will be presented in later reports, although we present some testing of these operators here. Our operator design utilizes group-theoretical projections. The point and space groups we use are well known, and the properties of their

irreducible representations are widely available in the literature. However, we collect together and present in this paper some of the specific group theory details needed for our operator construction for the convenience of the reader and as a record of our conventions and notation.

The Monte Carlo method commonly employed in QCD computations applies only to space-time lattices of finite extent. Hence, our goal is to obtain the stationary-state energies of QCD in a cubic box using periodic boundary conditions. In such a cubic box, we no longer have full rotational symmetry, even in the continuous space-time limit. The stationary states cannot be labeled by the usual spin- $J$  quantum numbers. Instead, the stationary states in a box with periodic boundary conditions must be labeled by the irreducible representations (irreps) of the cubic space group, even in the continuum limit.

This paper is organized as follows. Our approach to building single-hadron operators of definite momentum is described in Sec. II. We construct operators that transform irreducibly under all symmetries of a three-dimensional cubic lattice. Monte Carlo calculations are required to test our operator construction, and we present the implementation details of such computations in Sec. III. Tests of our single-hadron operators using the stochastic LapH method on  $24^3 \times 128$  and  $32^3 \times 256$  anisotropic lattices with pion masses  $m_\pi \approx 390$  and  $240$  MeV are then presented in Sec. IV. How we combine these operators to form two-hadron operators is described in Sec. V, and initial tests are presented. In Sec. VI, a new glueball operator is introduced and we demonstrate the feasibility of evaluating the mixing of this glueball operator with a quark-antiquark operator, an  $\eta\eta$  operator, and multiple two-pion operators. Concluding remarks are given in Sec. VII, along with our plans for future work.

## II. SINGLE-HADRON OPERATORS OF DEFINITE MOMENTUM

We extract the finite-volume stationary-state energies of QCD from matrices of temporal correlations  $C_{ij}(t_F - t_0) = \langle 0 | T O_i(t_F) \bar{O}_j(t_0) | 0 \rangle$ , where  $T$  denotes time ordering, the source operators  $\bar{O}_j(t_0)$  create the states of interest at an initial time  $t_0$ , and the sink operators  $O_i(t_F)$  annihilate the states of interest at a later time  $t_F$ . The correlation functions  $C_{ij}(t)$  can be expressed in terms of “path” integrals over quark fields  $\bar{\psi}, \psi$  and gluon fields  $U$  involving the QCD action having the form

$$S[\bar{\psi}, \psi, U] = \bar{\psi} K[U] \psi + S_G[U], \quad (1)$$

where  $K[U]$  is known as the Dirac matrix and  $S_G[U]$  is the gauge-field action. We use an anisotropic space-time lattice in which the temporal spacing  $a_t$  is smaller than the spacing  $a_s$  in the three spatial dimensions. Each time slice is a three-dimensional cubic lattice. We assume periodic boundary conditions in all three spatial directions. In order to estimate the path integrals using the

Monte Carlo method, it is necessary to work in the imaginary time formalism. This also has the advantage of converting oscillatory factors in real time into decaying exponentials. Our Euclidean space-time conventions, including the Euclidean Dirac  $\gamma$  matrices, are given in Ref. [1]. In the four-vector  $x_\mu$  describing a given lattice site, the  $\mu = 4$  component specifies the position in time, and the  $\mu = 1, 2, 3$  components specify the position along the Cartesian  $x, y, z$  spatial directions. As usual in lattice gauge theory, the gluon field is introduced using the parallel transporter  $U_\mu(x)$  given by the path-ordered exponential of the gauge field along a link in the  $\mu$  direction connecting neighboring sites of the lattice. The Dirac spinor field  $\psi_{a\alpha}^A(x)$  annihilates a quark and creates an antiquark at lattice site  $x$ , where  $A$  refers to the quark flavor,  $a$  refers to color, and  $\alpha$  is the Dirac spin index, and the field  $\bar{\psi}_{a\alpha}^A(x)$  annihilates an antiquark and creates a quark. Unlike in Minkowski space-time,  $\psi$  and  $\bar{\psi}$  must be treated as independent fields. When used in path integrals, the link variables are  $SU(3)$  matrices and  $\bar{\psi}, \psi$  are complex Grassmann fields.

Our hadron operators are constructed using spatially-smoothed link variables  $\tilde{U}_j(x)$  and spatially-smearred quark fields  $\tilde{\psi}(x)$ . The spatial links are smeared using the stout-link procedure described in Ref. [25]. Note that only spatial staples are used in the link smoothening; no temporal staples are used. The smeared quark field for each quark flavor is defined by

$$\tilde{\psi}_{a\alpha}(x) = \mathcal{S}_{ab}(x, y) \psi_{b\alpha}(y), \quad (2)$$

where  $x, y$  are lattice sites,  $a, b$  are color indices, and  $\alpha$  is a Dirac spin component. We use the Laplacian Heaviside (LapH) quark-field smearing scheme introduced in Ref. [26] and defined by

$$\mathcal{S} = \Theta(\sigma_s^2 + \tilde{\Delta}), \quad (3)$$

where  $\tilde{\Delta}$  is the three-dimensional gauge-covariant Laplacian defined in terms of the stout-smearred gauge field  $\tilde{U}$ , and  $\sigma_s$  is the smearing cutoff parameter. More details concerning this smearing scheme are described in Ref. [6].

All of our single-hadron operators are assemblages of basic building blocks which are gauge-covariantly-displaced, LapH-smearred quark fields:

$$q_{a\alpha j}^A = D^{(j)} \tilde{\psi}_{a\alpha}^{(A)}, \quad \bar{q}_{a\alpha j}^A = \tilde{\bar{\psi}}_{a\alpha}^{(A)} \gamma_4 D^{(j)\dagger}, \quad (4)$$

where  $a$  is a color index,  $\alpha$  is a Dirac spin component,  $A$  is a quark flavor,  $\gamma_4$  is the temporal Dirac  $\gamma$  matrix, and  $D^{(j)}$  is a gauge-covariant displacement of type  $j$ . The displacement type is a sequence of  $p$  spatial directions on the lattice  $j = (j_1, j_2, \dots, j_p)$ . This displacement can be trivial ( $j = 0$  meaning no displacement), a displacement in a given single spatial direction on the lattice by some number of links (typically two or three), or a combination of two or

more spatial lattice directions. If we define  $d_r = \hat{j}_1 + \hat{j}_2 + \dots + \hat{j}_{r-1}$ , then the displacement  $D^{(j)}$  is defined as a product of smeared link variables:

$$D^{(j)}(x, x') = \tilde{U}_{j_1}(x) \tilde{U}_{j_2}(x + d_2) \tilde{U}_{j_3}(x + d_3) \cdots \times \tilde{U}_{j_p}(x + d_p) \delta_{x', x+d_{p+1}}. \quad (5)$$

The use of  $\gamma_4$  in Eq. (4) is convenient for obtaining baryon correlation matrices that are Hermitian. To simplify notation, the Dirac spin component and the displacement type are sometimes combined into a single index in what follows.

We can simplify our spectrum calculations as much as possible by working with single-hadron operators that transform irreducibly under all symmetries of a three-dimensional cubic lattice of infinite extent or finite extent with periodic boundary conditions. Such symmetries form the simple cubic space group known as  $O_h^1$  in Schönflies notation or  $\text{Pm}\bar{3}\text{m}$  in international notation. This crystallographic space group is a semidirect product of the Abelian group of allowed translations on a simple cubic lattice and the orthogonal point group  $O_h$ . For bosonic systems with zero strangeness, we add  $G$  parity as a symmetry operation.

In order to construct such hadron operators, we first need to identify all of the symmetry operations and to determine how our basic building blocks transform under these operations. An element of the space group  $O_h^1$  is here denoted by  $(R, \mathbf{b})$ , where  $R$  is a spatial rotation or reflection about the origin and is an element of the point group  $O_h$ , and  $\mathbf{b}$  is an allowed spatial shift. The group element  $(R, \mathbf{b})$  corresponds to the coordinate transformation  $\mathbf{x} \rightarrow R\mathbf{x} + \mathbf{b}$ . The covariantly-displaced quark fields transform according to

$$U_{(R, \mathbf{b})} q_{a\alpha j}^A(\mathbf{x}) U_{(R, \mathbf{b})}^\dagger = S(R)_{\alpha\beta}^{-1} q_{a\beta Rj}^A(R\mathbf{x} + \mathbf{b}), \quad (6)$$

$$U_{(R, \mathbf{b})} \bar{q}_{a\alpha j}^A(\mathbf{x}) U_{(R, \mathbf{b})}^\dagger = \bar{q}_{a\beta Rj}^A(R\mathbf{x} + \mathbf{b}) S(R)_{\beta\alpha}, \quad (7)$$

where  $U_{(R, \mathbf{b})}$  denotes the quantum field operator that effects the transformation  $(R, \mathbf{b})$ , and the transformation matrices for spatial inversion  $I_s$  and proper rotations  $C_{nj}$  through angle  $2\pi/n$  about axis  $Oj$  are given by

$$S(C_{nj}) = \exp\left(\frac{1}{8} \omega_{\mu\nu} [\gamma_\mu, \gamma_\nu]\right), \quad (8)$$

$$S(I_s) = \gamma_4, \quad (9)$$

with  $\omega_{kl} = -2\pi\epsilon_{jkl}/n$  and  $\omega_{4k} = \omega_{k4} = 0$  ( $\omega_{\mu\nu}$  is an antisymmetric tensor which parametrizes rotations and boosts). A rotation by  $\pi/2$  about the  $y$  axis is conventionally denoted by  $C_{4y}$ , and  $C_{4z}$  denotes a rotation by  $\pi/2$  about the  $z$  axis. These particular group elements are given by

$$S(C_{4y}) = \frac{1}{\sqrt{2}}(1 + \gamma_1\gamma_3), \quad S(C_{4z}) = \frac{1}{\sqrt{2}}(1 + \gamma_2\gamma_1). \quad (10)$$

The allowed rotations on a three-dimensional spatially-isotropic cubic lattice form the octahedral group  $O$  which has 24 elements. For the convenience of the reader, the rotation axes corresponding to these group elements are shown in Fig. 1. Inclusion of spatial inversion  $I_s$  yields the point group  $O_h$  which has 48 elements occurring in ten conjugacy classes. All elements of  $O_h$  can be generated from appropriate products of only  $C_{4y}$ ,  $C_{4z}$ , and  $I_s$ . Under  $G$  parity, our basic building blocks transform according to

$$U_G q_{a\alpha j}^A(x) U_G^\dagger = \bar{q}_{a\beta j}^B(x) (\gamma_2)_{\beta\alpha} G^{BA}, \quad (11)$$

$$U_G \bar{q}_{a\alpha j}^A(x) U_G^\dagger = (\gamma_2)_{\alpha\beta} q_{a\beta j}^B(x) G^{BA}, \quad (12)$$

using the Dirac-Pauli representation for the  $\gamma$  matrices, and where the only nonzero elements of the  $G$  flavor matrix are  $G^{ud} = -G^{du} = -G^{ss} = 1$ .

The construction of irreducible representations (irreps) of  $O_h^1$  begins with the irreps of the Abelian subgroup of lattice translations. These are characterized by a definite three-momentum  $\mathbf{p}$  as allowed by the periodic boundary conditions.

Each of our meson operators which destroys a three-momentum  $\mathbf{p}$  is a linear superposition of gauge-invariant quark-antiquark elemental operators of the form

$$\Phi_{\alpha\beta}^{AB}(t) = \sum_{\mathbf{x}} e^{-i\mathbf{p}\cdot(\mathbf{x} + \frac{1}{2}(\mathbf{d}_\alpha + \mathbf{d}_\beta))} \delta_{ab} \bar{q}_{a\alpha}^A(\mathbf{x}, t) q_{b\beta}^B(\mathbf{x}, t), \quad (13)$$

where  $q, \bar{q}$  are defined in Eq. (4),  $\mathbf{d}_\alpha, \mathbf{d}_\beta$  are the spatial displacements of the  $\bar{q}, q$  fields, respectively, from  $\mathbf{x}$ ,  $A, B$  indicate flavor, and  $\alpha, \beta$  are compound indices incorporating both spin and quark-displacement types. The phase factor involving the quark-antiquark displacements is needed to ensure proper transformation properties under  $G$  parity for arbitrary displacement types. The ‘‘barred’’ operators which create a momentum  $\mathbf{p}$  then take the form

$$\bar{\Phi}_{\alpha\beta}^{AB}(t) = \sum_{\mathbf{x}} e^{i\mathbf{p}\cdot(\mathbf{x} + \frac{1}{2}(\mathbf{d}_\alpha + \mathbf{d}_\beta))} \delta_{ab} \bar{q}_{b\beta}^B(\mathbf{x}, t) q_{a\alpha}^A(\mathbf{x}, t). \quad (14)$$

Each meson sink operator has the form

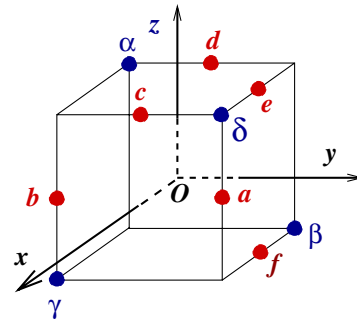


FIG. 1 (color online). The axes  $Ox, Oy, Oz, Oa, Ob, Oc, Od, Oe, Of, O\alpha, O\beta, O\gamma, O\delta$  corresponding to the group elements  $C_{nj}$  of the octahedral group  $O$ , where  $C_{nj}$  denotes a proper rotation through angle  $2\pi/n$  about axis  $Oj$ .

$$M_l(t) = c_{\alpha\beta}^{(l)} \Phi_{\alpha\beta}^{AB}(t) \quad (15)$$

(or is a flavor combination of the above form), where  $l$  is a compound index comprised of a three-momentum  $\mathbf{p}$ , an irreducible representation  $\Lambda$  of the little group of  $\mathbf{p}$  (discussed below), the row  $\lambda$  of the irrep, total isospin  $I$ , isospin projection  $I_3$ , strangeness  $S$ , and an identifier labeling the different operators in each symmetry channel. Here, we focus on mesons containing only  $u, d, s$  quarks. The corresponding source operators are

$$\bar{M}_l(t) = c_{\alpha\beta}^{(l)*} \bar{\Phi}_{\alpha\beta}^{AB}(t). \quad (16)$$

Each of our baryon operators destroying a three-momentum  $\mathbf{p}$  is a linear superposition of gauge-invariant elemental three-quark operators of the form

$$\Phi_{\alpha\beta\gamma}^{ABC}(\mathbf{p}, t) = \sum_{\mathbf{x}} e^{-i\mathbf{p}\cdot\mathbf{x}} \varepsilon_{abc} q_{a\alpha}^A(\mathbf{x}, t) q_{b\beta}^B(\mathbf{x}, t) q_{c\gamma}^C(\mathbf{x}, t). \quad (17)$$

The barred three-quark elemental operators which create a momentum  $\mathbf{p}$  have the form

$$\bar{\Phi}_{\alpha\beta\gamma}^{ABC}(\mathbf{p}, t) = \sum_{\mathbf{x}} e^{i\mathbf{p}\cdot\mathbf{x}} \varepsilon_{abc} \bar{q}_{c\gamma}^C(\mathbf{x}, t) \bar{q}_{b\beta}^B(\mathbf{x}, t) \bar{q}_{a\alpha}^A(\mathbf{x}, t). \quad (18)$$

Our baryon sink operators, being linear superpositions of the three-quark elemental operators, have the form



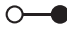




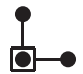

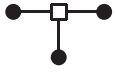

$$B_l(t) = c_{\alpha\beta\gamma}^{(l)} \Phi_{\alpha\beta\gamma}^{ABC}(t), \quad (19)$$

where again, the  $l$  label includes the momentum  $\mathbf{p}$ , the little group irrep  $\Lambda$ , the row  $\lambda$  of the irrep, isospin  $I$ , isospin projection  $I_3$ , strangeness  $S$ , and an identifier specifying the different operators in each symmetry channel. We focus on baryons containing only  $u, d, s$  quarks. The corresponding source operators are

$$\bar{B}_l(t) = c_{\alpha\beta\gamma}^{(l)*} \bar{\Phi}_{\alpha\beta\gamma}^{ABC}(t). \quad (20)$$

In order to build up the necessary orbital and radial structures expected in the hadron excitations, we use a variety of spatially-extended configurations for our hadron operators, as shown in Table I. First, consider the zero-momentum operators. The simplest meson operators combine the quark and antiquark fields at the same lattice site. We refer to these as single-site (SS) operators. In the singly-displaced (SD) meson operators, the quark is displaced from the antiquark along a direction parallel to one of the axes of the lattice. If the quark is covariantly displaced from the antiquark along an L-shaped path, we refer to this as a doubly-displaced-L operator. Displacement of the quark along a U-shaped path or in three orthogonal directions from the antiquark leads to triply-displaced-U and triply-displaced-O (TDO) meson operators, respectively, as shown in Table I. The simplest baryon operators combine the three quarks at a single lattice site. In the singly-displaced baryons, one of the quarks is displaced from the other two along a direction parallel to one of the

TABLE I. The spatial arrangements of the quark-antiquark meson operators (left) and the three-quark baryon operators (right). In the illustrations, the smeared quarks fields are depicted by solid circles, each hollow circle indicates a smeared barred antiquark field, the solid line segments indicate covariant displacements, and each hollow box indicates the location of a Levi-Civita color coupling. For simplicity, all displacements have the same length in an operator.

Meson configurations	Baryon configurations
	
single-site	single-site
	
singly-displaced	singly-displaced
	
doubly-displaced-L	doubly-displaced-I
	
triply-displaced-U	doubly-displaced-L
	
triply-displaced-O	triply-displaced-T
	
	triply-displaced-O

axes of the lattice. Displacement of two quarks away from the site of the Levi-Civita coupling leads to doubly-displaced-I and doubly-displaced-L baryon operators of zero momentum. All three quarks can be displaced from the color-coupling site, producing triply-displaced-T and triply-displaced-O baryon operators of zero momentum, as illustrated in Table I. For simplicity, all displacement lengths along each of the different directions are taken to be the same in any given operator. For mesons, we use a length of  $3a_s$ , and for baryons, the length is  $2a_s$ , as will be discussed later.

For nonzero momenta, we restrict our attention to on-axis momenta, such as in the  $\pm\hat{x}$ ,  $\pm\hat{y}$ ,  $\pm\hat{z}$  directions, to momenta in a planar-diagonal direction, such as  $\pm\hat{x} \pm \hat{y}$ ,  $\pm\hat{x} \pm \hat{z}$ ,  $\pm\hat{y} \pm \hat{z}$ , and momenta in a cubic-diagonal direction, such as  $\pm\hat{x} \pm \hat{y} \pm \hat{z}$ . We expect that the above momentum directions are sufficient for studying the stationary states in the range of energies of interest to us. For on-axis momenta, we construct single-site meson and baryon operators, longitudinally-singly-displaced (LSD) operators in which one quark is displaced along the direction of the momentum, and transverse-singly-displaced (TSD) operators, in which one quark is displaced along a direction of the lattice transverse to the momentum. For

planar-diagonal momenta, we use single-site meson and baryon operators, transverse-singly-displaced operators in which one quark is displaced along the direction of the lattice that is perpendicular to the plane containing the momentum direction, and planar-singly-displaced operators in which one quark is displaced along one of the two directions of the lattice coinciding with the nonzero components of the momentum. For cubic-diagonal momenta, we use single-site and singly-displaced (SD) configurations for both baryons and mesons. For such momenta, displacements along the lattice axes are neither entirely transverse nor entirely longitudinal to the momentum. For mesons, we also use triply-displaced-O (TDO) operators for the on-axis, planar-diagonal, and cubic-diagonal momenta.

For a given flavor structure, the next step in our single-hadron operator construction is to find coefficients in Eqs. (15) and (19) that produce operators which transform irreducibly under all symmetries of the three-dimensional cubic lattice. First, for each class of momenta, such as on axis or planar diagonal, we choose one representative reference momentum direction  $\mathbf{p}_{\text{ref}}$ . We then find coefficients corresponding to operators that transform irreducibly under the little group of  $\mathbf{p}_{\text{ref}}$ . Recall that the little group of  $\mathbf{p}_{\text{ref}}$  is the subset of symmetry operations that leave the reference momentum  $\mathbf{p}_{\text{ref}}$  invariant. Next, for each momentum direction  $\mathbf{p}$  in a class of momenta, we select one reference rotation  $R_{\text{ref}}^{\mathbf{p}}$  that transforms  $\mathbf{p}_{\text{ref}}$  into  $\mathbf{p}$ . As long as the selected group element transforms  $\mathbf{p}_{\text{ref}}$  into  $\mathbf{p}$ , it does not matter which group element is chosen, but a choice must be made and clearly specified. Hadron operators having a momentum in the direction of  $\mathbf{p}$  are then obtained by applying the reference rotation to the operators constructed using the momentum in the direction of  $\mathbf{p}_{\text{ref}}$ . Our choices of reference momenta directions and reference rotations are listed in Table II.

Our choices of reference directions and rotations, as well as our choices of the irreducible representation matrices, described later, are dictated mainly by simplicity. An alternate approach would be to choose the  $z$  direction as the single reference direction, obtain all other momenta using a rotation defined by the Jacob-Wick convention, and use irreducible representation matrices corresponding to helicity states. Since our procedure for combining the single-hadron operators into multihadron operators is automated using MAPLE, we found that there was no great advantage in using the standard Jacob-Wick convention with helicities.

The little groups associated with our choices of reference momentum directions are listed in Tables III, IV, V, and VI. To describe both mesons and baryons, we need the single-valued and double-valued (spinorial) irreps of these groups. The double-valued representations of a group  $\mathcal{G}$  are constructed by extending the group elements to form the so-called ‘‘double group’’  $\mathcal{G}^D$ . This is done by

TABLE II. Our choices for the reference momentum  $\mathbf{p}_{\text{ref}}$  directions and the reference rotations  $R_{\text{ref}}$  for each momentum  $\mathbf{p}$  direction that we use.

$\mathbf{p}_{\text{ref}}$ direction	$\mathbf{p}$ direction	$R_{\text{ref}}^{\mathbf{p}}$	
(0,0,1)	(0, 0, -1)	$C_{2x}$	
	(1,0,0)	$C_{4y}$	
	(-1, 0, 0)	$C_{4y}^{-1}$	
	(0, -1, 0)	$C_{4x}$	
	(0, 1, 0)	$C_{4x}^{-1}$	
	(0,1,1)	(0, -1, -1)	$C_{2x}$
		(0, 1, -1)	$C_{4x}^{-1}$
		(0, -1, 1)	$C_{4x}$
		(1,0,1)	$C_{4z}^{-1}$
		(-1, 0, -1)	$C_{2b} = C_{2x}C_{4z}$
(1, 0, -1)		$C_{2a} = C_{2y}C_{4z}$	
(1,1,1)	(-1, 0, 1)	$C_{4z}$	
	(1,1,0)	$C_{4y}$	
	(-1, -1, 0)	$C_{2d} = C_{2z}C_{4y}$	
	(1, -1, 0)	$C_{2c} = C_{4y}C_{2z}$	
	(-1, 1, 0)	$C_{4y}^{-1}$	
	(1, 1, -1)	$C_{4y}$	
	(1, -1, 1)	$C_{4x}$	
	(1, -1, -1)	$C_{2x}$	
	(-1, 1, 1)	$C_{4z}$	
	(-1, 1, -1)	$C_{2y}$	
(1,1,1)	(-1, -1, 1)	$C_{2z}$	
	(-1, -1, -1)	$C_{2d} = C_{2z}C_{4y}$	

introducing a new generator, denoted by  $\bar{E}$ , which represents a rotation by  $2\pi$  about any axis. For each element  $G$  of the original group, the double group contains another element  $\bar{G} = \bar{E}G$ . For the convenience of the reader, the elements of the double groups associated with our choices of reference momentum directions are explicitly listed in Tables III, IV, V, and VI, grouped into their conjugacy classes.

TABLE III. The little group corresponding to reference momentum direction (0,0,0) is  $O_h$ . The elements of the double group  $O_h^D$  are listed below, grouped into conjugacy classes.  $E$  is the identity element,  $\bar{E}$  represents a rotation by  $2\pi$  about any axis, and  $\bar{G} = \bar{E}G$  for each element  $G$  in  $O_h$ . Spatial inversion  $I_s$  in  $O_h^D$  satisfies  $I_s^2 = E$  and  $I_s^{-1} = I_s$ . Conjugacy classes  $C_9$  through  $C_{16}$  are not listed below. The elements of class  $C_{n+8}$  are obtained by multiplying each of the elements in class  $C_n$  by  $I_s$ .

$C_1 = \{E\}$
$C_2 = \{C_{3\alpha}, C_{3\beta}, C_{3\gamma}, C_{3\delta}, C_{3\alpha}^{-1}, C_{3\beta}^{-1}, C_{3\gamma}^{-1}, C_{3\delta}^{-1}\}$
$C_3 = \{C_{2x}, C_{2y}, C_{2z}, \bar{C}_{2x}, \bar{C}_{2y}, \bar{C}_{2z}\}$
$C_4 = \{C_{4x}, C_{4y}, C_{4z}, C_{4x}^{-1}, C_{4y}^{-1}, C_{4z}^{-1}\}$
$C_5 = \{C_{2a}, C_{2b}, C_{2c}, C_{2d}, C_{2e}, C_{2f}, \bar{C}_{2a}, \bar{C}_{2b}, \bar{C}_{2c}, \bar{C}_{2d}, \bar{C}_{2e}, \bar{C}_{2f}\}$
$C_6 = \{\bar{E}\}$
$C_7 = \{\bar{C}_{3\alpha}, \bar{C}_{3\beta}, \bar{C}_{3\gamma}, \bar{C}_{3\delta}, \bar{C}_{3\alpha}^{-1}, \bar{C}_{3\beta}^{-1}, \bar{C}_{3\gamma}^{-1}, \bar{C}_{3\delta}^{-1}\}$
$C_8 = \{\bar{C}_{4x}, \bar{C}_{4y}, \bar{C}_{4z}, \bar{C}_{4x}^{-1}, \bar{C}_{4y}^{-1}, \bar{C}_{4z}^{-1}\}$

TABLE IV. The little group corresponding to reference momentum direction (0,0,1) is  $C_{4v}$ . The elements of the double group  $C_{4v}^D$  for this reference momentum direction are listed below, grouped into conjugacy classes.  $E$  is the identity element,  $\bar{E}$  represents a rotation by  $2\pi$  about any axis.

$C_1 = \{E\}$
$C_2 = \{C_{2z}, \bar{C}_{2z}\}$
$C_3 = \{C_{4z}, C_{4z}^{-1}\}$
$C_4 = \{I_s C_{2x}, I_s C_{2y}, I_s \bar{C}_{2x}, I_s \bar{C}_{2y}\}$
$C_5 = \{I_s C_{2a}, I_s C_{2b}, I_s \bar{C}_{2a}, I_s \bar{C}_{2b}\}$
$C_6 = \{\bar{E}\}$
$C_7 = \{\bar{C}_{4z}, \bar{C}_{4z}^{-1}\}$

TABLE V. The little group corresponding to reference momentum direction (0,1,1) is  $C_{2v}$ . The elements of the double group  $C_{2v}^D$  for this reference momentum direction are listed below, grouped into conjugacy classes.

$C_1 = \{E\}$
$C_2 = \{C_{2e}, \bar{C}_{2e}\}$
$C_3 = \{I_s C_{2f}, I_s \bar{C}_{2f}\}$
$C_4 = \{I_s C_{2x}, I_s \bar{C}_{2x}\}$
$C_5 = \{\bar{E}\}$

The irreducible representations of these little groups and their characters are listed in Tables VII, VIII, IX, and X. One-dimensional single-valued irreps are labeled by  $A$  or  $B$ , two-dimensional irreps are denoted by  $E$ , and three-dimensional irreps are labeled by  $T$ . One-dimensional double-valued irreps are denoted by  $F$ , two-dimensional spinor irreps are denoted by  $G$ , and four-dimensional irreps are indicated by  $H$ . A subscript  $g$  indicates an even-parity irrep, whereas a subscript  $u$  indicates an odd-parity irrep. For mesons which are eigenstates of  $G$  parity, a “+” superscript indicates an irrep describing states even under  $G$  parity, and a “−” superscript indicates an irrep associated with states odd under  $G$  parity. Our notation differs from that of Refs. [27,28].

Our method of constructing the hadron operators that transform irreducibly under each little group makes use of group-theoretical projections and is described in detail in Ref. [1]. The first step in the method is to identify a basis of hadron elemental operators  $\Phi_i(t)$  at a single time  $t$  that

TABLE VI. The little group corresponding to reference momentum direction (1,1,1) is  $C_{3v}$ . The elements of the double group  $C_{3v}^D$  are listed below, grouped into conjugacy classes.

$C_1 = \{E\}$
$C_2 = \{C_{3\delta}, C_{3\delta}^{-1}\}$
$C_3 = \{I_s C_{2b}, I_s C_{2d}, I_s C_{2f}\}$
$C_4 = \{\bar{E}\}$
$C_5 = \{\bar{C}_{3\delta}, \bar{C}_{3\delta}^{-1}\}$
$C_6 = \{I_s \bar{C}_{2b}, I_s \bar{C}_{2d}, I_s \bar{C}_{2f}\}$

TABLE VII. Characters  $\chi^\Lambda$  of the single-valued and double-valued irreducible representations  $\Lambda$  of the group  $O_h$ . Only the even-parity irreps (subscript  $g$ ) and classes  $C_1$  to  $C_8$  are shown below. For the even-parity irreps,  $\chi_{n+8}^\Lambda = \chi_n^\Lambda$ , where  $\chi_n^\Lambda$  denotes the character of  $\Lambda$  for all group elements in class  $C_n$ . For the odd-parity irreps (subscript  $u$  instead of  $g$ ),  $\chi_n^{\Lambda^u} = \chi_n^{\Lambda^g}$  for  $n = 1 \dots 8$ , and  $\chi_n^{\Lambda^u} = -\chi_n^{\Lambda^g}$  for  $n = 9 \dots 16$ .

$\Lambda$	$\chi_1^\Lambda$	$\chi_2^\Lambda$	$\chi_3^\Lambda$	$\chi_4^\Lambda$	$\chi_5^\Lambda$	$\chi_6^\Lambda$	$\chi_7^\Lambda$	$\chi_8^\Lambda$
$A_{1g}$	1	1	1	1	1	1	1	1
$A_{2g}$	1	1	1	-1	-1	1	1	-1
$E_g$	2	-1	2	0	0	2	-1	0
$T_{1g}$	3	0	-1	1	-1	3	0	1
$T_{2g}$	3	0	-1	-1	1	3	0	-1
$G_{1g}$	2	1	0	$\sqrt{2}$	0	-2	-1	$-\sqrt{2}$
$G_{2g}$	2	1	0	$-\sqrt{2}$	0	-2	-1	$\sqrt{2}$
$H_g$	4	-1	0	0	0	-4	1	0

TABLE VIII. Characters  $\chi^\Lambda$  for the single-valued and double-valued irreps  $\Lambda$  of the group  $C_{4v}$ .

$\Lambda$	$\chi_1^\Lambda$	$\chi_2^\Lambda$	$\chi_3^\Lambda$	$\chi_4^\Lambda$	$\chi_5^\Lambda$	$\chi_6^\Lambda$	$\chi_7^\Lambda$
$A_1$	1	1	1	1	1	1	1
$A_2$	1	1	1	-1	-1	1	1
$B_1$	1	1	-1	1	-1	1	-1
$B_2$	1	1	-1	-1	1	1	-1
$E$	2	-2	0	0	0	2	0
$G_1$	2	0	$\sqrt{2}$	0	0	-2	$-\sqrt{2}$
$G_2$	2	0	$-\sqrt{2}$	0	0	-2	$\sqrt{2}$

transform into one another under the elements of the little group  $\mathcal{G}$ . The key formula in obtaining the linear combinations  $O_i$  of these basis operators that transform irreducibly under  $\mathcal{G}$  is

$$O_i^{\Lambda}(t) = \frac{d_\Lambda}{g_{\mathcal{G}^D}} \sum_{R \in \mathcal{G}^D} \Gamma_{\lambda\lambda}^{(\Lambda)}(R) U_R \Phi_i(t) U_R^\dagger, \quad (21)$$

where  $\mathcal{G}^D$  is the double group of  $\mathcal{G}$ ,  $R$  denotes an element of  $\mathcal{G}^D$ ,  $g_{\mathcal{G}^D}$  is the number of elements in  $\mathcal{G}^D$ ,  $d_\Lambda$  is the dimension of the  $\Lambda$  irreducible representation, and  $\Gamma^\Lambda(R)$  is the matrix for element  $R$  in irrep  $\Lambda$ .

To carry out the projections in Eq. (21), explicit representation matrices  $\Gamma$  are needed for each group element,

TABLE IX. Characters  $\chi^\Lambda$  for the single-valued and double-valued irreps  $\Lambda$  of the group  $C_{2v}$ .

$\Lambda$	$\chi_1^\Lambda$	$\chi_2^\Lambda$	$\chi_3^\Lambda$	$\chi_4^\Lambda$	$\chi_5^\Lambda$
$A_1$	1	1	1	1	1
$A_2$	1	1	-1	-1	1
$B_1$	1	-1	1	-1	1
$B_2$	1	-1	-1	1	1
$G$	2	0	0	0	-2

TABLE X. Characters  $\chi^\Lambda$  for the single-valued and double-valued irreps  $\Lambda$  of the group  $C_{3v}$ .

$\Lambda$	$\chi_1^\Lambda$	$\chi_2^\Lambda$	$\chi_3^\Lambda$	$\chi_4^\Lambda$	$\chi_5^\Lambda$	$\chi_6^\Lambda$
$A_1$	1	1	1	1	1	1
$A_2$	1	1	-1	1	1	-1
$E$	2	-1	0	2	-1	0
$F_1$	1	-1	$i$	-1	1	$-i$
$F_2$	1	-1	$-i$	-1	1	$i$
$G$	2	1	0	-2	-1	0

and a representation for the Dirac  $\gamma$  matrices must be selected. We use the Dirac-Pauli representation for the  $\gamma$  matrices, as described in Ref. [1]. Often, helicity states are used for moving hadrons in continuous space-time. We could find no great advantage in using a helicity representation for our subsequent lattice calculations involving multihadron operators. The use of helicity states does not result in any reduction in the number of irrep rows that must be evaluated for the single moving hadron states. All of our group theory manipulations are implemented using MAPLE, so the computational effort is independent of our choices of representation matrices. Instead, we chose the simplest possible matrices for our irreducible representations. Our choices of representation matrices are summarized in Tables XI, XII, XIII, and XIV. The representation

matrices for all group elements can be obtained by suitable multiplications of the matrices shown in these tables.

For a given set of elemental hadron operators that transform among one another, many of the projections in Eq. (21) vanish or lead to linearly-dependent operators, so the final step in the operator construction is to choose suitable linear combinations of the projected operators to obtain a final set of independent single-hadron operators. These linear combinations are obtained using a Gram-Schmidt procedure as described in Ref. [1].

At the end of this entire procedure, we obtain single-hadron annihilation operators  $B_{p\Lambda\lambda i}^{I_3 S}$  characterized by total isospin  $I$ , the projection of the total isospin  $I_3$ , strangeness  $S$ , momentum  $\mathbf{p}$ , little group irrep  $\Lambda$ , and irrep row  $\lambda$ . Here, we use the index  $i$  to indicate all other quantum numbers and identifying information. All of these single-hadron operators constructed as described above transform under a group element  $(R, \mathbf{b})$  of the space group  $O_h^1$ , in which  $\mathbf{x} \rightarrow R\mathbf{x} + \mathbf{b}$ , according to

$$U_{(R,\mathbf{b})} B_{p\Lambda\lambda i}^{I_3 S}(t) U_{(R,\mathbf{b})}^\dagger = B_{Rp\Lambda\mu i}^{I_3 S}(t) \Gamma_{\mu\lambda}^{(\Lambda)}(R_W^p)^* e^{i\mathbf{b}\cdot R\mathbf{p}}, \quad (22)$$

$$U_{(R,\mathbf{b})} \bar{B}_{p\Lambda\lambda i}^{I_3 S}(t) U_{(R,\mathbf{b})}^\dagger = \bar{B}_{Rp\Lambda\mu i}^{I_3 S}(t) \Gamma_{\mu\lambda}^{(\Lambda)}(R_W^p) e^{-i\mathbf{b}\cdot R\mathbf{p}},$$

where the Wigner rotation is given by

$$R_W^p = (R_{\text{ref}}^p)^{-1} R R_{\text{ref}}^p, \quad (23)$$

TABLE XI. Our choices for the representation matrices  $\Gamma$  of the single-valued and double-valued irreps  $\Lambda$  of the group  $O_h$  for zero momentum operators. Only the even-parity irreps (subscript  $g$ ) are shown below. The matrices for  $C_{4y}$  and  $C_{4z}$  for the odd-parity irreps (subscript  $u$ ) are the same. Spatial inversion  $I_s$  is the third generator.  $\Gamma^{(\Lambda)}(I_s)$  is the identity matrix for the even-parity irreps, and minus one times the identity for the odd-parity irreps. The matrices for all other group elements can be obtained from appropriate multiplications of the matrices below and the matrix for  $I_s$ .

$\Lambda$	$\Gamma^{(\Lambda)}(C_{4y})$	$\Gamma^{(\Lambda)}(C_{4z})$
$A_{1g}$	[1]	[1]
$A_{2g}$	[-1]	[-1]
$E_g$	$\frac{1}{2} \begin{bmatrix} 1 & \sqrt{3} \\ \sqrt{3} & -1 \end{bmatrix}$	$\begin{bmatrix} -1 & 0 \\ 0 & 1 \end{bmatrix}$
$T_{1g}$	$\begin{bmatrix} 0 & 0 & 1 \\ 0 & 1 & 0 \\ -1 & 0 & 0 \end{bmatrix}$	$\begin{bmatrix} 0 & -1 & 0 \\ 1 & 0 & 0 \\ 0 & 0 & 1 \end{bmatrix}$
$T_{2g}$	$\begin{bmatrix} 0 & 0 & -1 \\ 0 & -1 & 0 \\ 1 & 0 & 0 \end{bmatrix}$	$\begin{bmatrix} 0 & 1 & 0 \\ -1 & 0 & 0 \\ 0 & 0 & -1 \end{bmatrix}$
$G_{1g}$	$\frac{1}{\sqrt{2}} \begin{bmatrix} 1 & -1 \\ 1 & 1 \end{bmatrix}$	$\frac{1}{\sqrt{2}} \begin{bmatrix} 1-i & 0 \\ 0 & 1+i \end{bmatrix}$
$G_{2g}$	$\frac{-1}{\sqrt{2}} \begin{bmatrix} 1 & -1 \\ 1 & 1 \end{bmatrix}$	$\frac{-1}{\sqrt{2}} \begin{bmatrix} 1-i & 0 \\ 0 & 1+i \end{bmatrix}$
$H_g$	$\frac{1}{2\sqrt{2}} \begin{bmatrix} 1 & -\sqrt{3} & \sqrt{3} & -1 \\ \sqrt{3} & -1 & -1 & \sqrt{3} \\ \sqrt{3} & 1 & -1 & -\sqrt{3} \\ 1 & \sqrt{3} & \sqrt{3} & 1 \end{bmatrix}$	$\frac{1}{\sqrt{2}} \begin{bmatrix} -1-i & 0 & 0 & 0 \\ 0 & 1-i & 0 & 0 \\ 0 & 0 & 1+i & 0 \\ 0 & 0 & 0 & -1+i \end{bmatrix}$

TABLE XII. Our choices for the representation matrices  $\Gamma$  of the single-valued and double-valued irreps  $\Lambda$  of the little group  $C_{4v}$  for momentum in the direction (0,0,1). The matrices for all other group elements can be obtained from appropriate multiplications of the matrices below.

$\Lambda$	$\Gamma^{(\Lambda)}(C_{4z})$	$\Gamma^{(\Lambda)}(I_s C_{2y})$
$A_1$	[1]	[1]
$A_2$	[1]	[-1]
$B_1$	[-1]	[1]
$B_2$	[-1]	[-1]
$E$	$\begin{bmatrix} 0 & -1 \\ 1 & 0 \end{bmatrix}$	$\begin{bmatrix} 1 & 0 \\ 0 & -1 \end{bmatrix}$
$G_1$	$\frac{1}{\sqrt{2}} \begin{bmatrix} 1-i & 0 \\ 0 & 1+i \end{bmatrix}$	$\begin{bmatrix} 0 & -1 \\ 1 & 0 \end{bmatrix}$
$G_2$	$\frac{-1}{\sqrt{2}} \begin{bmatrix} 1-i & 0 \\ 0 & 1+i \end{bmatrix}$	$\begin{bmatrix} 0 & -1 \\ 1 & 0 \end{bmatrix}$

TABLE XIII. Our choices for the representation matrices  $\Gamma$  of the single-valued and double-valued irreps  $\Lambda$  of the little group  $C_{2v}$  for momentum in the direction (0,1,1). The matrices for all other group elements can be obtained from appropriate multiplications of the matrices below.  $C_{2e} = C_{2z}C_{4x}$  is a rotation about (0,1,1), and  $C_{2f} = C_{2y}C_{4x}$  is a rotation about (0, 1, -1).

$\Lambda$	$\Gamma^{(\Lambda)}(C_{2e})$	$\Gamma^{(\Lambda)}(I_s C_{2f})$
$A_1$	[1]	[1]
$A_2$	[1]	[-1]
$B_1$	[-1]	[1]
$B_2$	[-1]	[-1]
$G$	$\frac{1}{\sqrt{2}} \begin{bmatrix} -i & -1 \\ 1 & i \end{bmatrix}$	$\frac{1}{\sqrt{2}} \begin{bmatrix} i & -1 \\ 1 & -i \end{bmatrix}$

and is an element of the little group of  $\mathbf{p}$ . Note that the above equations apply even when  $R$  refers to spatial inversion  $I_s$ . Equations (22) and (23) play a crucial role when forming the multihadron operators. The behaviors of our operators under  $G$  parity and isospin rotations are considered below.

TABLE XIV. Our choices for the representation matrices  $\Gamma$  of the single-valued and double-valued irreps  $\Lambda$  of the little group  $C_{3v}$  for momentum in the direction (1,1,1). The matrices for all other group elements can be obtained from appropriate multiplications of the matrices below.  $C_{3\delta} = C_{4y}C_{4z}$  is a rotation about (1,1,1), and  $C_{2b} = C_{2x}C_{4z}$  is a rotation about (1, -1, 0).

$\Lambda$	$\Gamma^{(\Lambda)}(C_{3\delta})$	$\Gamma^{(\Lambda)}(I_s C_{2b})$
$A_1$	[1]	[1]
$A_2$	[1]	[-1]
$E$	$\frac{1}{2} \begin{bmatrix} -1 & \sqrt{3} \\ -\sqrt{3} & -1 \end{bmatrix}$	$\begin{bmatrix} -1 & 0 \\ 0 & 1 \end{bmatrix}$
$F_1$	[-1]	[i]
$F_2$	[-1]	[-i]
$G$	$\frac{1}{2} \begin{bmatrix} 1-i & -1-i \\ 1-i & 1+i \end{bmatrix}$	$\frac{1}{\sqrt{2}} \begin{bmatrix} 0 & 1-i \\ -1-i & 0 \end{bmatrix}$

In Ref. [1], the odd-parity zero-momentum baryons were constructed from their even-parity partner operators utilizing a particular transformation involving charge conjugation. For a given even-parity zero-momentum baryon operator  $B_i^g(t)$ , an odd-parity operator  $B_i^u(t)$  can be defined by rotating the three Dirac indices using the  $\gamma_2$  matrix and replacing the expansion coefficients by their complex conjugates. This yields particular relationships between the temporal correlation matrices of the even-parity baryons and the time-reversed correlation matrices of the odd-parity baryon operators, allowing averaging over forward and backward temporal propagations in some cases for increased statistics. However, for the baryon operators having nonzero momentum, parity is no longer a good quantum number since it reverses the three-momentum. For this reason, we do not bother to apply a generalization of the above procedure in constructing the odd-parity baryon operators of nonzero momentum, especially since the increased statistical precision can be obtained in other more efficient ways when using the stochastic LapH method.

In constructing our light pion and kaon operators, we take symmetry under time reversal into account. Although the lattices we use are rather large in temporal extent, temporal wrap-around effects can still come into play for the light pions and kaons in certain situations where high precision is needed, such as in studying the  $\pi\pi$  scattering phase shifts. Energies can be extracted with increased statistical precision if meson operators whose temporal correlations are symmetric under time reversal are used. Symmetry under time reversal helps in extracting meson energies whenever temporal wrap-around effects become non-negligible since the functional forms used for fitting the data have fewer parameters, leading to more precise energy estimates. For meson operators, the energies of the states propagating backwards in time are the same as those of the states traveling forwards in time, but the couplings of a given meson operator to the forward-propagating states can differ from the couplings to the backward-propagating states if symmetry under time reversal is not taken into account.

We can reduce the number of needed fit parameters if we use meson operators whose temporal correlation matrices satisfy  $C_{\mu\nu}(t) = C_{\mu\nu}(N_t - t)$ , where  $N_t$  is the temporal extent of the lattice, assuming periodic boundary conditions in time. This can be achieved if each meson operator itself satisfies  $M_i(t) = \eta M_i(N_t - t)$ , with  $|\eta|^2 = 1$ . Under a certain symmetry of the lattice action that involves time reversal, the covariantly-displaced LapH-smearred quark fields transform according to

$$\begin{aligned} q_{\alpha\beta}^A(x) &\rightarrow (\gamma_4\gamma_5)_{\alpha\beta} q_{\alpha\beta}^A(\mathcal{T}x), \\ \bar{q}_{\alpha\beta}^A(x) &\rightarrow \bar{q}_{\alpha\beta}^A(\mathcal{T}x)(\gamma_4\gamma_5)_{\beta\alpha}, \end{aligned} \quad (24)$$

where  $(\mathcal{T}x)_j = x_j$  and  $(\mathcal{T}x)_4 = N_t - x_4$ . Since wrap-around effects are a potential problem only for the lightest mesons, we decided to modify only the symmetry channels containing the lightest pseudoscalars ( $\pi, K, \eta$ ). In each



case, we projected the operators into the even and odd operators under the above transformation. Numerical tests using a small number of configurations showed that the odd operators performed somewhat better, but the difference was not very significant. Hence, we discarded the even operators, and kept the odd operators. Note that the operator  $\bar{\psi}\gamma_5\psi$  is odd under the above transformation.

As in Ref. [1], we work in the approximation that the masses of the  $u$  and  $d$  quarks are equal, and we neglect electromagnetic interactions. In this approximation, the theory has an exact isotopic spin symmetry, and states are characterized by total isospin  $I$ , its projection  $I_3$  onto a given axis, and strangeness  $S$ . Again, we consider only the  $u, d, s$  quarks here. Incorporating this isospin symmetry into our operators is straightforward and has been described in Ref. [1]. The flavor structure of the hadron operators we use is summarized in Table XV. Due to an approximate  $SU(3)$   $uds$ -flavor symmetry, quark flavor combinations in meson and baryon operators are often chosen according to the irreducible representations of  $SU(3)$  flavor. Such combinations are simply linear superpositions of the operators presented in Table XV. Since we plan to obtain Monte Carlo estimates of the complete correlation matrices of operators including all allowed flavor combinations, the use of linear superpositions which transform irreducibly under  $SU(3)$  flavor is unnecessary.

TABLE XV. Flavor structure of the elemental hadron annihilation operators we use. Each is characterized by isospin  $I$ , maximal  $I_3 = I$ , strangeness  $S$ , and  $G$  parity, where applicable, expressed in terms of the gauge-invariant three-quark and quark-antiquark operators defined in Eqs. (17) and (13), respectively.  $U_G$  is the quantum operator that effects a  $G$ -parity transformation. Recall that  $f, f', h, h', b, a$  are even-parity mesons, while  $\eta, \eta', \omega, \phi, \rho, \pi$  are odd-parity mesons. Also, a flavored meson is named  $K^*$  if its total spin  $J$  and parity  $P$  are both odd or both even, otherwise it is named  $K$ .

Hadron	$I = I_3$	$S$	$G$	Annihilation operators
$\Delta^{++}$	$\frac{3}{2}$	0		$\Phi_{\alpha\beta\gamma}^{uuu}$
$\Sigma^+$	1	-1		$\Phi_{\alpha\beta\gamma}^{uus}$
$N^+$	$\frac{1}{2}$	0		$\Phi_{\alpha\beta\gamma}^{uud} - \Phi_{\alpha\beta\gamma}^{duu}$
$\Xi^0$	$\frac{1}{2}$	-2		$\Phi_{\alpha\beta\gamma}^{ssu}$
$\Lambda^0$	0	-1		$\Phi_{\alpha\beta\gamma}^{uds} - \Phi_{\alpha\beta\gamma}^{dus}$
$\Omega^-$	0	-3		$\Phi_{\alpha\beta\gamma}^{sss}$
$f, f', \eta, \eta'$	0	0	1	$\Phi_{\alpha\beta}^{uu} + \Phi_{\alpha\beta}^{dd} + U_G(\Phi_{\alpha\beta}^{uu} + \Phi_{\alpha\beta}^{dd})U_G^\dagger$ $\Phi_{\alpha\beta}^{ss} + U_G\Phi_{\alpha\beta}^{ss}U_G^\dagger$
$h, h', \omega, \phi$	0	0	-1	$\Phi_{\alpha\beta}^{uu} + \Phi_{\alpha\beta}^{dd} - U_G(\Phi_{\alpha\beta}^{uu} + \Phi_{\alpha\beta}^{dd})U_G^\dagger$ $\Phi_{\alpha\beta}^{ss} - U_G\Phi_{\alpha\beta}^{ss}U_G^\dagger$
$b^+, \rho^+$	1	0	1	$\Phi_{\alpha\beta}^{du} + U_G\Phi_{\alpha\beta}^{du}U_G^\dagger$
$a^+, \pi^+$	1	0	-1	$\Phi_{\alpha\beta}^{du} - U_G\Phi_{\alpha\beta}^{du}U_G^\dagger$
$K^+, K^{*+}$	$\frac{1}{2}$	1		$\Phi_{\alpha\beta}^{su}$
$\bar{K}^0, \bar{K}^{*0}$	$\frac{1}{2}$	-1		$\Phi_{\alpha\beta}^{ds}$

TABLE XVI. Continuum limit spin identification: the number  $n_\Lambda^J$  of times that the  $\Lambda$  single-valued irrep of the octahedral point group  $O_h$  occurs in the (reducible) subduction of the integer  $J$  irrep of  $SU(2)$ . The numbers for  $A_{1u}, A_{2u}, E_u, T_{1u}, T_{2u}$  are the same as for  $A_{1g}, A_{2g}, E_g, T_{1g}, T_{2g}$ , respectively.

$J$	$n_{A_{1g}}^J$	$n_{A_{2g}}^J$	$n_{E_g}^J$	$n_{T_{1g}}^J$	$n_{T_{2g}}^J$
0	1	0	0	0	0
1	0	0	0	1	0
2	0	0	1	0	1
3	0	1	0	1	1
4	1	0	1	1	1
5	0	0	1	2	1
6	1	1	1	1	2
7	0	1	1	2	2
8	1	0	2	2	2
9	1	1	1	3	2

For example, we construct isoscalar meson operators having flavor content  $\bar{u}u + \bar{d}d$  separately from those having flavor content  $\bar{s}s$ . Our correlation matrices then allow mixings of these operators. Our choices of operators described in Table XV are dictated by computational simplicity. In summary, we construct single-hadron operators that transform under an isospin rotation  $R_\tau$  according to

$$U_{R_\tau} B_{p\Lambda\lambda i}^{I_3 S}(t) U_{R_\tau}^\dagger = B_{p\Lambda\lambda i}^{I_3 S}(t) D_{I_3' I_3}^{(I)}(R_\tau)^*, \quad (25)$$

$$U_{R_\tau} \bar{B}_{p\Lambda\lambda i}^{I_3 S}(t) U_{R_\tau}^\dagger = \bar{B}_{p\Lambda\lambda i}^{I_3 S}(t) D_{I_3' I_3}^{(I)}(R_\tau),$$

where  $D^{(I)}(R_\tau)$  are the familiar Wigner rotation matrices. Our meson operators  $M$  are constructed such that they transform under  $G$  parity according to

$$U_G M_{p\Lambda\lambda i}^{I_3 S}(t) U_G^\dagger = \eta_\Lambda M_{p\Lambda\lambda i}^{I_3, -S}(t), \quad (26)$$

$$U_G \bar{M}_{p\Lambda\lambda i}^{I_3 S}(t) U_G^\dagger = \eta_\Lambda \bar{M}_{p\Lambda\lambda i}^{I_3, -S}(t),$$

where  $\eta_\Lambda = 1$  if  $S = \pm 1$ , and when the strangeness  $S = 0$ , then  $\eta_\Lambda = \pm 1$  depending on the  $G$ -parity superscript of the irrep  $\Lambda$ .

To associate our finite-box energies with observed hadrons, it is necessary to know which spin- $J$  irreps of the continuous group of rotations occur in which irreps of

TABLE XVII. Continuum limit spin identification: the number  $n_\Lambda^J$  of times that the  $\Lambda$  double-valued irrep of the octahedral point group  $O_h$  occurs in the (reducible) subduction of the half-integral  $J$  irrep of  $SU(2)$ . The numbers for  $G_{1u}, G_{2u}, H_u$  are the same as for  $G_{1g}, G_{2g}, H_g$ , respectively.

$J$	$n_{G_{1g}}^J$	$n_{G_{2g}}^J$	$n_{H_g}^J$	$J$	$n_{G_{1g}}^J$	$n_{G_{2g}}^J$	$n_{H_g}^J$
$\frac{1}{2}$	1	0	0	$\frac{9}{2}$	1	0	2
$\frac{3}{2}$	0	0	1	$\frac{11}{2}$	1	1	2
$\frac{5}{2}$	0	1	1	$\frac{13}{2}$	1	2	2
$\frac{7}{2}$	1	1	1	$\frac{15}{2}$	1	1	3

TABLE XVIII. Subduction  $\downarrow$  of the irreducible representations of  $O_h$  to the irreducible representations of the little groups  $C_{4v}$ ,  $C_{3v}$ , and  $C_{2v}$ .

$\Lambda(O_h)$	$\downarrow C_{4v}$	$\downarrow C_{3v}$	$\downarrow C_{2v}$
$A_{1g}$	$A_1$	$A_1$	$A_1$
$A_{1u}$	$A_2$	$A_2$	$A_2$
$A_{2g}$	$B_1$	$A_2$	$B_2$
$A_{2u}$	$B_2$	$A_1$	$B_1$
$E_g$	$A_1 \oplus B_1$	$E$	$A_1 \oplus B_2$
$E_u$	$A_2 \oplus B_2$	$E$	$A_2 \oplus B_1$
$T_{1g}$	$A_2 \oplus E$	$A_2 \oplus E$	$A_2 \oplus B_1 \oplus B_2$
$T_{1u}$	$A_1 \oplus E$	$A_1 \oplus E$	$A_1 \oplus B_1 \oplus B_2$
$T_{2g}$	$B_2 \oplus E$	$A_1 \oplus E$	$A_1 \oplus A_2 \oplus B_1$
$T_{2u}$	$B_1 \oplus E$	$A_2 \oplus E$	$A_1 \oplus A_2 \oplus B_2$
$G_{1g/u}$	$G_1$	$G$	$G$
$G_{2g/u}$	$G_2$	$G$	$G$
$H_{g/u}$	$G_1 \oplus G_2$	$F_1 \oplus F_2 \oplus G$	$2G$

TABLE XIX. The irreducible representations of  $O_h$  in which various commonly-known hadrons at rest occur.

Hadron	Irrep	Hadron	Irrep	Hadron	Irrep
$\pi$	$A_{1u}^-$	$K$	$A_{1u}$	$\eta, \eta'$	$A_{1u}^+$
$\rho$	$T_{1u}^+$	$\omega, \phi$	$T_{1u}^-$	$K^*$	$T_{1u}$
$a_0$	$A_{1g}^+$	$f_0$	$A_{1g}^+$	$h_1$	$T_{1g}^-$
$b_1$	$T_{1g}^+$	$K_1$	$T_{1g}$	$\pi_1$	$T_{1u}^-$
$N, \Sigma$	$G_{1g}$	$\Lambda, \Xi$	$G_{1g}$	$\Delta, \Omega$	$H_g$

the octahedral point group. For the convenience of the reader, the spin contents of the  $O_h$  single-valued and double-valued irreps are listed in Tables XVI and XVII, respectively. These tables list the number of times that each irrep  $\Lambda$  of  $O_h$  appears in various  $J$  irreps of  $SU(2)$  subduced to the double group of  $O_h$ . Table XVIII is useful for identifying which hadrons of nonzero momentum appear in which irreps of the little groups. The decompositions of the subduced representations of  $O_h$  into the irreps of the little groups  $C_{4v}$ ,  $C_{3v}$ , and  $C_{2v}$  are given in this table. Table XIX lists the irreps of  $O_h$  in which various common hadrons at rest appear.

### III. IMPLEMENTATION DETAILS

In order to test the effectiveness of the single-hadron operators that we have designed, Monte Carlo calculations must be carried out. Details on how the temporal correlations of hadron operators are evaluated using Monte Carlo integration with the stochastic LapH method are presented in this section. Many of these details have already been described in Ref. [6], so only details in addition to those in Ref. [6] are presented here, along with some reiteration of important run parameters.

Our computations use the so-called stochastic LapH method [6] and are done in a sequence of steps:

(a) generation of gauge-field configurations using the Monte Carlo method; (b) computation of quark sinks for various noises and dilution projectors using the configurations from the first step; (c) computation of the single meson and single baryon sources and sinks using the quark sources and sinks from the second step; (d) evaluation of the correlators using the single-hadron sources and sinks and their combinations into multihadron sources and sinks; and (e) analysis of the correlators to extract the energies. These steps are discussed below.

A description of step (a) is given in Ref. [29]. We are currently focusing on three Monte Carlo ensembles: (A) a set of 412 gauge-field configurations on a large  $32^3 \times 256$  anisotropic lattice with a pion mass  $m_\pi \sim 240$  MeV, (B) an ensemble of 551 configurations on an  $24^3 \times 128$  anisotropic lattice with a pion mass  $m_\pi \sim 390$  MeV, and (C) an ensemble of 584 configurations on an  $24^3 \times 128$  anisotropic lattice with a pion mass  $m_\pi \sim 240$  MeV. We refer to these ensembles as the  $(32^3|240)$ ,  $(24^3|390)$ , and  $(24^3|240)$  ensembles, respectively. These ensembles were generated using the Rational Hybrid Monte Carlo (RHMC) algorithm [30], which is a Metropolis method with a sophisticated means of proposing a global change to the gauge and pseudofermion fields. A fictitious momentum is introduced for each link variable with a Gaussian distribution, and a Hamiltonian is formed involving these momenta and the original action as a potential energy. A new field configuration is proposed by approximately solving Hamilton's equations for some length of fictitious time, known as an RHMC trajectory. In each ensemble, successive configurations are separated by 20 RHMC trajectories to minimize autocorrelations. An improved anisotropic clover fermion action and an improved gauge field action are used [29]. In these ensembles,  $\beta = 1.5$  and the  $s$  quark mass parameter is set to  $m_s = -0.0743$  in order to reproduce a specific combination of hadron masses [29]. In the  $(24^3|390)$  ensemble, the light quark mass parameters are set to  $m_u = m_d = -0.0840$  so that the pion mass is around 390 MeV if one sets the scale using the  $\Omega$  baryon mass. In the  $(32^3|240)$  and  $(24^3|240)$  ensembles,  $m_u = m_d = -0.0860$  are used, resulting in a pion mass around 240 MeV. The spatial grid size is  $a_s \sim 0.12$  fm, whereas the temporal spacing is  $a_t \sim 0.035$  fm.

A description of step (b) above, computation of the quark sinks, is given in Ref. [6]. We employ the Laplacian Heaviside quark-field smearing scheme defined using the three-dimensional gauge-covariant Laplacian expressed in terms of a stout-smear gauge field. The spatial links are smeared using the stout-link procedure described in Ref. [25] with  $n_\xi = 10$  iterations and staple weight  $\xi = 0.10$ . For the cutoff in the LapH smearing, we use  $\sigma_s^2 = 0.33$ , which translates into the number  $N_v$  of LapH eigenvectors retained being  $N_v = 112$  for the  $24^3$  lattices and  $N_v = 264$  for the  $32^3$  lattice. We use  $Z_4$  noise in all of our stochastic estimates of quark propagation. Our variance

reduction procedure is similar to that described in Ref. [31]. Our noise dilution projectors are products of time dilution, spin dilution, and LapH eigenvector dilution projectors. We use a triplet (T, S, L) to specify a given dilution scheme, where ‘‘T’’ denotes time, ‘‘S’’ denotes spin, and ‘‘L’’ denotes LapH eigenvector dilution. The schemes are denoted by 1 for no dilution, F for full dilution, and BK and IK for block- $K$  and interlace- $K$ , respectively (see Ref. [6]). For all forward-time quark lines connecting source time  $t_0$  to the later sink time  $t_F$ , we use the dilution scheme (TF, SF, LI $j$ ), where  $j = 8$  for mesons and  $j = 4$  for baryons. We chose  $j = 4$  for baryons in order to dramatically reduce the disk space needed to store the baryon sources/sinks by a factor of 8. We found that the statistical errors in the baryon effective masses only increased by a factor of 2 in changing from LI8 to LI4. Given the eightfold reduction in both storage and computing time, we deemed this an acceptable loss of accuracy. For all same-sink-time  $t_F$ -to- $t_F$  quark lines, the dilution scheme (TI16, SF, LI $j$ ) is used, where  $j = 8$  for mesons and  $j = 4$  for baryons. The TI16 interlacing in time enables us to evaluate quark lines that originate on *any* time slice, allowing us to evaluate all diagrams needed to obtain the temporal correlations involving single-hadron and multi-hadron operators. Four widely-separated source times  $t_0$  are used on each  $24^3$  gauge configuration, whereas eight  $t_0$  values are used on the  $32^3$  lattice.

Details about how the single-hadron sources and sinks are computed in step (c) above can be found in Ref. [6]. A comprehensive survey of the spectrum of excited states in QCD requires obtaining temporal correlations of a large number of different operators. For example,  $K\bar{K}$  operators must mix with  $\pi\pi$  operators, and so on. Hence, a large variety of single-hadron operators must be available in the study of each sector, and a plethora of Wick contractions must be evaluated. In order to study all stationary states of QCD involving the  $u, d, s$  quarks, we need suitable sources and sinks for all isovector mesons ( $\pi, \rho, a, b$ ), all isoscalar mesons ( $\eta, f, h, \omega, \phi$ ), and all kaons. To study  $\bar{K}K$  states, we also need separate antikaon sources and sinks. For the isoscalar mesons, separate  $\bar{u}u + \bar{d}d$  and  $\bar{s}s$  operators are evaluated, and these will be allowed to mix in the correlation matrices. We also need all single-baryon  $N, \Delta, \Xi, \Lambda, \Sigma, \Omega$  sources and sinks. Each hadron source and sink involves a summation over color indices and the spatial sites on each time slice of the lattice. Different spin components and displacement directions are combined to form the hadron operators which transform irreducibly under the symmetry operations of the spatial lattice.

Using the lowest-lying energies in each symmetry sector as determined from low-statistics runs on small  $16^3$  lattices, we systematically identified all momenta in the different little group irreps that would be needed to capture the energy spectrum up to  $0.5a_t^{-1}$ , where  $a_t$  is the temporal lattice spacing. This energy value ensures that a sufficient

TABLE XX. The numbers  $N_{\text{op}}$  of single-hadron operators whose sinks and sources have been computed. The operator numbers include operators having zero, on-axis, planar-diagonal, and cubic-diagonal momenta, as well as momenta for the pions in various special directions, such as (0,1,2) and (1,1,2).  $N_{\text{mom}}$  indicates the number of momenta in the operator sets. Here,  $\pi$  refers to *any* isovector quark-antiquark meson operator with flavor content such as  $\bar{d}u$  (such as  $a, b, \pi$ , and  $\rho$  mesons),  $\eta$  refers to any  $\bar{u}u + \bar{d}d$  isoscalar meson operator,  $\phi$  refers to any  $\bar{s}s$  isoscalar meson operator,  $K$  refers to any quark-antiquark operator having flavor content  $\bar{s}u$  or  $\bar{s}d$  such that its strangeness is  $S = 1$ , and  $\bar{K}$  is any quark-antiquark operator having flavor content  $\bar{u}s$  or  $\bar{d}s$  such that its strangeness is  $S = -1$ .

	(24 <sup>3</sup>  390)		(24 <sup>3</sup>  240)		(32 <sup>3</sup>  240)	
	$N_{\text{op}}$	$N_{\text{mom}}$	$N_{\text{op}}$	$N_{\text{mom}}$	$N_{\text{op}}$	$N_{\text{mom}}$
$\pi$	1776	123	2028	123	2740	149
$\eta$	2012	51	2204	51	3078	77
$\phi$	2012	51	2204	51	3078	77
$K$	1499	51	1517	51	1949	65
$\bar{K}$	1499	51	1517	51	1949	65
$N/\Delta$	1472	33	...	...	1616	59
$\Lambda/\Sigma$	2274	33	...	...	2054	51
$\Xi$	1320	33	...	...	700	51
$\Omega$	728	33	...	...	680	45

number of hadrons accessible to experiments can be studied without overwhelming the computational resources available to us. The numbers  $N_{\text{op}}$  of single-hadron operators whose sinks and sources have been computed are listed in Table XX. The operator numbers include operators having zero, on-axis, planar-diagonal, and cubic-diagonal momenta, as well as momenta for pions in various special directions, such as (0,1,2) and (1,1,2).  $N_{\text{mom}}$  indicates the number of momenta in the operator sets. These operators were chosen from much larger sets. Small-volume, low-statistics runs were done to select operators having lower statistical noise and smaller contamination from higher-lying eigenstates. In this table,  $\pi$  refers to *any* isovector quark-antiquark meson operator with flavor content such as  $\bar{d}u$  (such as  $a, b, \pi$ , and  $\rho$  mesons),  $\eta$  refers to any  $\bar{u}u + \bar{d}d$  isoscalar meson operator,  $\phi$  refers to any  $\bar{s}s$  isoscalar meson operator,  $K$  refers to any quark-antiquark operator having flavor content  $\bar{s}u$  or  $\bar{s}d$  such that its strangeness is  $S = 1$ , and  $\bar{K}$  is any quark-antiquark operator having flavor content  $\bar{u}s$  or  $\bar{d}s$  such that its strangeness is  $S = -1$ . The  $N$  and  $\Delta$  were computed simultaneously, and so were the  $\Lambda$  and  $\Sigma$ , since these baryons share many of the same three-quark components.

Our final correlation matrices will not use such large numbers of operators. We will combine the single-hadron operators into two- and three-particle operators, projected into the irreps of the  $O_h$  point group. A last round of operator selections will then occur. Many of the multi-hadron operators will not produce signals of suitable quality or be linearly dependent with other operators. We will

have to identify a final set of multihadron operators that best allows us to extract the low-lying energy spectrum in each symmetry sector.

For baryons containing identical quark flavors, the sources/sinks defined by Eq. (23) in Ref. [6] can be evaluated by assigning the quark spin and displacement indices to the identical-flavor quark lines using either a single canonical one-to-one mapping or by averaging over all such one-to-one mappings. Averaging over the quark-line mappings is tantamount to averaging over different noises, so a reduction in the correlator variances can occur. However, operators of this form have more three-quark terms in them, and the resulting increase in the number of

“elemental” three-quark operators that must be evaluated raises the computational costs. We did some small lattice studies to compare the benefits/cost of the two different ways of assigning spin and displacement indices to the identical-flavor quark lines. We decided that the modest increase in computational cost was warranted, given the variance reduction that resulted.

Since our hadrons are made out of spatially-displaced quark fields, we carried out a study of the role of the displacement length in the meson and baryon operators. Excited-state contamination in the correlators of various meson and baryon operators was investigated for a range of displacement lengths. For the value of  $a_s \sim 0.12$  fm in the

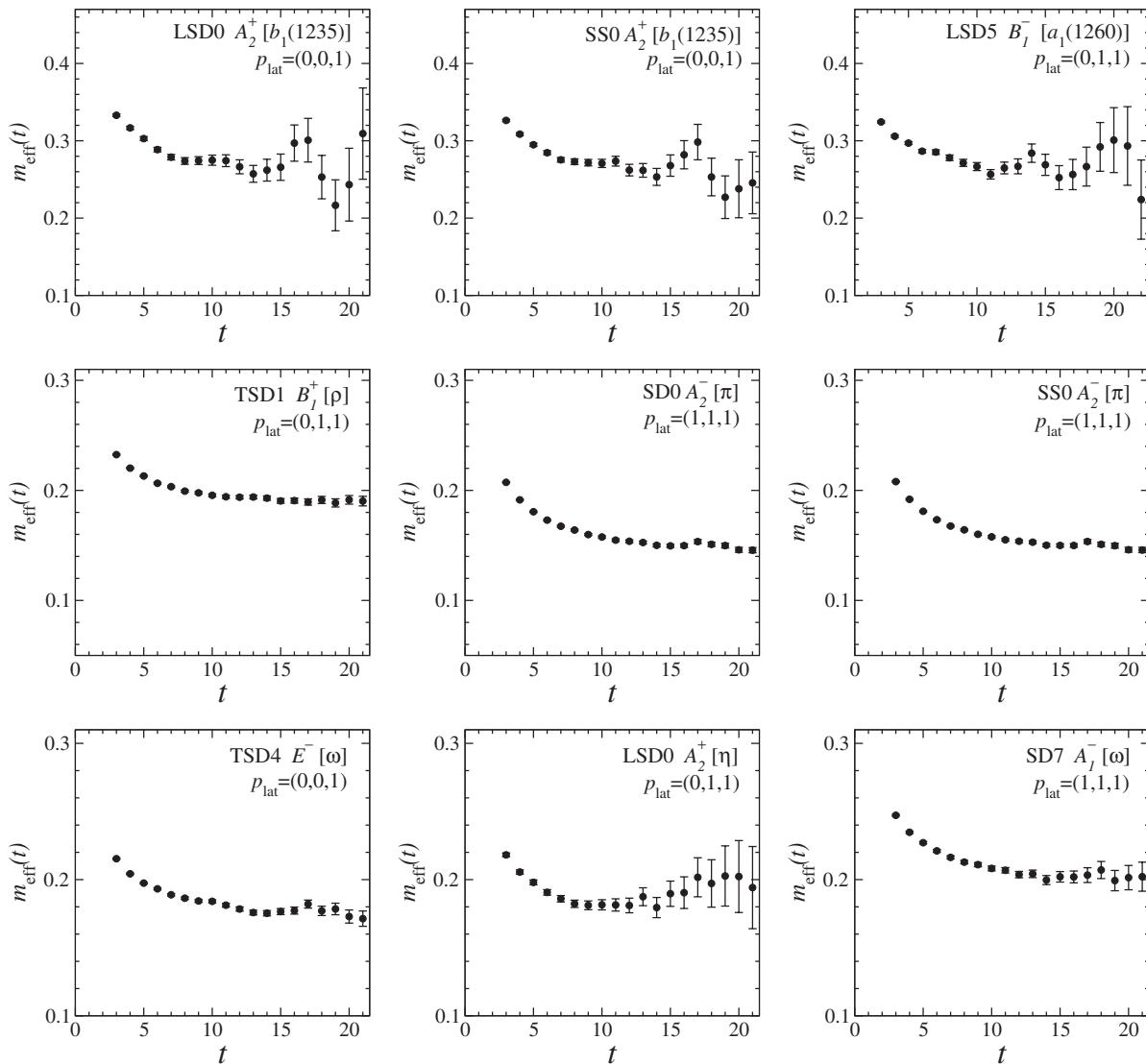


FIG. 2. Effective masses,  $m_{\text{eff}}(t)$  using  $dt = 3$ , associated with several isovector and isoscalar meson operators of various momenta  $\mathbf{p} = (2\pi/L)\mathbf{p}_{\text{lat}}$  on the  $(24^3)390$  ensemble, where  $L = 24a_s$  is the spatial extent of the lattice. SS refers to a single-site meson operator, and LSD denotes an operator in which the quark is displaced from the antiquark in a longitudinal direction along the direction of the momentum, as explained in Sec. II. In a TSD operator, the quark is displaced in a direction transverse to that of the momentum. For cubic-diagonal momenta, SD denotes a singly-displaced operator. The numbers following the letters, such as in SS0, are simply identifying integer indices. Particle names in the square brackets have been included to lend context to the little group irrep labels.

ensembles used, a displacement length of  $3a_s$  produced operators having somewhat better overlaps with the low-lying mesons of interest, whereas displacement lengths  $2a_s$  and  $3a_s$  worked well for baryons. Our conclusions concerning these lengths were found to be insensitive to changes in the quark-field smearing, although we did not study this in too much detail. These displacements can be rather costly for baryons, so we decided to use  $2a_s$  for all baryon operators. In addition to achieving overlaps with the states of interest, another concern in setting the displacement length is to obtain operators that are sufficiently different from one another to produce correlation matrices with reasonable condition numbers.

An outline of how the temporal correlations are obtained from the hadron sources and sinks, step (d) above, is given in Ref. [6]. First, thousands of single-hadron operators having different momenta for different noises, dilution schemes, and types of quark line ends [source or sink, normal mode or  $\gamma_5$  Hermitian conjugate mode using Eq. (17) in Ref. [6]] are evaluated and stored. The second task in step (d) is computing the temporal correlations using expressions such as Eqs. (24) and (33) in Ref. [6]. Given the large number of correlators that we will need to evaluate, it is important to automate the Wick contraction process as much as possible. MAPLE is used to create the software for the numerical evaluations. The first step in the MAPLE calculations is forming appropriate flavor combinations of symbolic Grassmann variables representing single-hadron and multihadron operators of definite total isospin  $I$ , strangeness  $S$ , and isospin projection  $I_3$ , raising and lowering the isospin projections of the individual constituent hadrons as needed. Next, the MAPLE code carries out the actual Wick contractions in terms of the Grassmann symbols. Finally, our MAPLE program outputs the C++ subroutines for use in numerically evaluating the correlators in terms of the stored hadron sources and sinks

in the different flavor sectors. In evaluating the individual quark-line diagrams, we apply  $\gamma_5$  Hermiticity [see Eq. (16) in Ref. [6]] in cases where a  $\psi(t_0)$  at the source connects with a  $\bar{\psi}(t_F)$  at the sink. For all same-time quark lines, we average over estimates obtained using both Eqs. (15) and (16) in Ref. [6] to increase statistics.

#### IV. TESTS OF THE SINGLE-HADRON OPERATORS

In order to test the effectiveness of the single-hadron operators that we have designed, we examined the effective masses associated with the correlators of a variety of meson and baryon operators having various momenta. Samples of these effective masses are shown in Figs. 2 and 3. In these figures, we use the following definition of the effective mass:

$$m_{\text{eff}}(t) = -\frac{1}{dt} \ln \left( \frac{C(t+dt)}{C(t)} \right), \quad (27)$$

where time separation  $t$  in the correlator  $C(t)$  is measured in term of the temporal lattice spacing  $a_t$ , and usually  $dt = 3$  is used.

Figure 2 shows the effective masses,  $m_{\text{eff}}(t)$  using  $dt = 3$ , associated with several isovector and isoscalar meson operators of various momenta  $\mathbf{p} = (2\pi/L)\mathbf{p}_{\text{lat}}$  on the  $(24^3|390)$  ensemble, where  $L = 24a_s$  is the spatial extent of the lattice. SS refers to a single-site meson operator, and LSD denotes an operator in which the quark is displaced from the antiquark in a longitudinal direction along the direction of the momentum, as explained in Sec. II. In a TSD operator, the quark is displaced in a direction transverse to that of the momentum. Several different operators of each spatial type can be constructed, and we label these different operators using an integer that varies from zero to the number of such operators less one. This integer is placed at the end of the spatial type label,

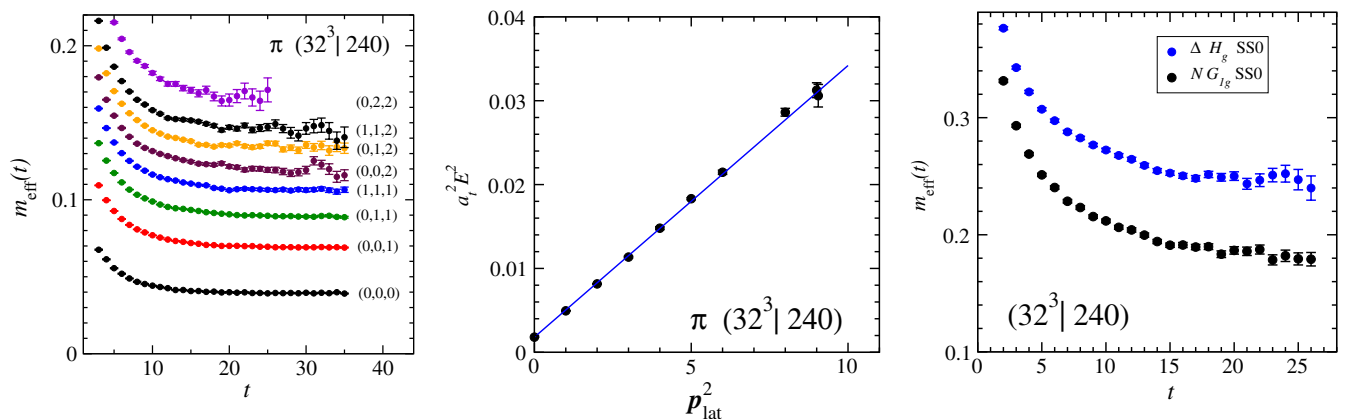


FIG. 3 (color online). Pion and baryon results obtained using the  $(32^3|240)$  ensemble. (Left) Effective masses,  $m_{\text{eff}}(t)$  using  $dt = 3$ , against temporal separation  $t$ , associated with single-site pion operators having different momenta. Each effective mass is labeled by its  $\mathbf{p}_{\text{lat}}$ . (Center) Dispersion relation for the pion showing  $a_t^2 E^2$  against  $\mathbf{p}_{\text{lat}}^2$ , where  $E$  is the pion energy. (Right) Effective masses,  $m_{\text{eff}}(t)$  using  $dt = 3$ , against temporal separation  $t$ , associated with two single-site baryon operators having zero momentum. One effective mass corresponds to the nucleon ( $G_{1g}$  channel) and the other to a  $\Delta$  baryon ( $H_g$  channel).

such as SS0 or TSD4. Results for on-axis momentum  $\mathbf{p}_{\text{lat}} = (0, 0, 1)$ , planar-diagonal momentum  $\mathbf{p}_{\text{lat}} = (0, 1, 1)$ , and cubic-diagonal momentum  $\mathbf{p}_{\text{lat}} = (1, 1, 1)$  are shown. The names of the lowest-lying known particles which appear in these finite-volume symmetry channels are indicated in square brackets.

Energies of the pion, nucleon, and  $\Delta$ , obtained using the  $(32^3|240)$  ensemble, are studied in Fig. 3. In the left plot, effective masses associated with single-site pion operators having different momenta are shown against temporal separation  $t$  using  $dt = 3$ . Each effective mass is labeled by its  $\mathbf{p}_{\text{lat}}$ . The dispersion relation for the pion is shown in the center plot, which displays  $a_7^2 E^2$  against  $\mathbf{p}_{\text{lat}}^2$ , where  $E$  is the pion energy. Effective masses associated with two single-site baryon operators having zero momentum are shown in the right plot of Fig. 3. One effective mass corresponds to the nucleon ( $G_{1g}$  channel) and the other to a  $\Delta$  baryon ( $H_g$  channel).

Both Figs. 2 and 3 show that the stochastic LapH method works well for moving hadrons on large lattices. These plots also confirm that our choices of the gauge-field and quark-field smearing parameters and our noise dilution schemes for reducing variances are suitable for treating hadron states having nonzero definite momenta on the three Monte Carlo ensembles we plan to use.

## V. TWO-HADRON OPERATORS OF DEFINITE MOMENTUM

We construct our two-hadron operators using the same procedure described in Sec. II to build the single-hadron operators, except that the basic building blocks are now the single-hadron operators instead of the elemental three-quark and quark-antiquark operators. This procedure allows us to very efficiently build up the many multihadron

operators that our spectrum computations will need. Evaluating the single-hadron sources and sinks of various momenta requires summations over both quark color and spin indices, as well as summations over the spatial sites of the lattice. Once these relatively expensive computations are done for the single hadrons, the multihadron operators, being simple linear combinations of the single-hadron operators, are very inexpensive to compute, and many of them can be quickly made.

In addition to efficiency, there are good physical reasons for using such multihadron operators. Hadron-hadron interactions in finite volume move the energies of any two-hadron systems away from their free two-particle energies, and the interacting two-particle states could involve distributions of different relative momenta. However, such interactions are usually small and the relative momenta used in our operators should presumably dominate in most cases. Also, we will always utilize multihadron operators with a variety of different relative momenta to accommodate the effects of such interactions. The performance of some of our  $\pi\pi$  operators are compared to localized multihadron operators in Fig. 4, discussed below.

Each single-hadron operator is labeled by total isospin  $I$ , the projection of the total isospin  $I_3$ , strangeness  $S$ , three-momentum  $\mathbf{p}$ , the little group irrep  $\Lambda$ , the row of the irrep  $\lambda$ , and  $i$ , which denotes all other identifying information, such as the displacement type and index. Hence, basis operators for the two-hadron operators can be written

$$B_{\mathbf{p}_a \Lambda_a \lambda_a i_a}^{I_a I_{3a} S_a} B_{\mathbf{p}_b \Lambda_b \lambda_b i_b}^{I_b I_{3b} S_b}, \quad (28)$$

where  $B$  denotes either a baryon (as a Grassmann operator) or a meson, and  $a$  and  $b$  denote the separate hadrons. Although the above operators form a perfectly acceptable basis of operators, they do not transform irreducibly

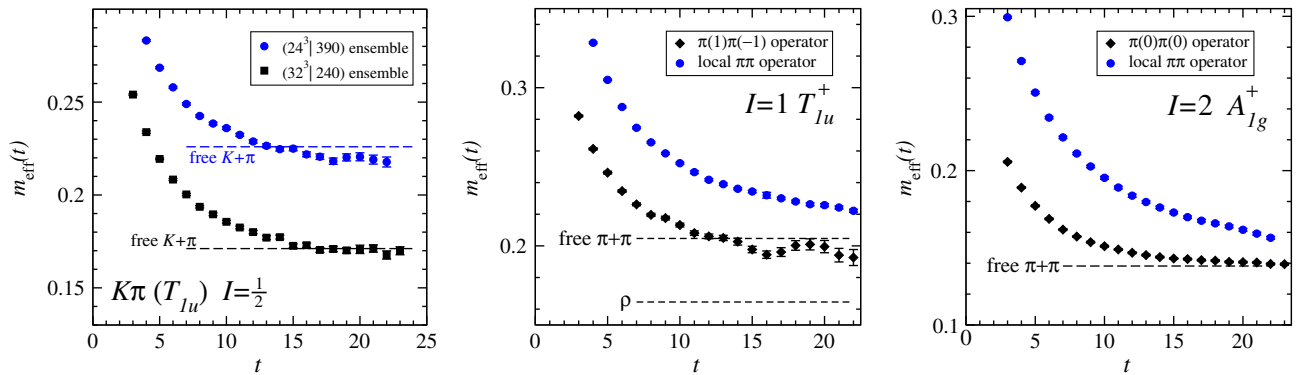


FIG. 4 (color online). (Left) Effective masses,  $m_{\text{eff}}(t)$  using  $dt = 3$ , associated with a two-meson operator in the  $T_{1u}$  irrep, having total isospin  $I = \frac{1}{2}$  and zero total momentum, constructed from single-site kaon and pion operators having equal and opposite on-axis momenta of minimal nonzero magnitude. Results on the  $(24^3|390)$  and  $(32^3|240)$  ensembles are shown. The energies of a free  $\pi$  plus a free  $K$  are indicated by horizontal dashed lines. (Center) Effective mass for one of our  $I = 1$   $\pi(1)\pi(-1)$  operators in the  $T_{1u}^+$  channel, consisting of single-site pion operators having equal and opposite on-axis momenta of minimal nonzero magnitude, compared to the effective mass of a localized  $\pi\pi$  operator, described in Eq. (30), on the  $(24^3|390)$  ensemble. (Right) Effective mass for one of our  $I = 2$   $\pi(0)\pi(0)$  operators in the  $A_{1g}^+$  channel, consisting of single-site pion operators each having zero momenta, compared to the effective mass of a localized  $\pi\pi$  operator, described in Eq. (29), on the  $(24^3|390)$  ensemble.

under isospin rotations, nor under the  $O_h^1$  symmetry transformations.

To construct such irreducible operators, we first need to know how the basis operators transform. Equations (22), (23), (25), and (26) summarize the important transformation properties of our single-hadron operators. Starting with the basis operators above, we first identify subsets of these operators that transform among themselves under all  $O_h^1$  transformations. The total momentum  $\mathbf{p} = \mathbf{p}_a + \mathbf{p}_b$  is the first quantity we consider. We identify the little group of transformations that leave  $\mathbf{p}$  invariant, then our goal is to construct operators that transform according to the  $\Lambda$  irrep of that little group. Under group element  $R$  of  $O_h^1$ , the single particle operator  $B_{\mathbf{p}_a \Lambda_a \lambda_a i_a}^{I_a T_{3a} S_a}$  transforms into one that has possibly a different momentum  $R\mathbf{p}_a$  and is a linear combination of the different rows of the  $\Lambda_a$  irrep. The following quantities do not change under the  $O_h^1$  transformations:  $\Lambda_a$ ,  $\Lambda_b$ ,  $i_a$ ,  $i_b$ . We fix the above quantities, then apply the same group-theoretical projections as for the single-hadrons to construct the linear combinations that transform irreducibly. This can be easily done since we know exactly how each of the basis operators transforms under any  $O_h^1$  transformation. Next, we form flavor combinations that transform irreducibly under isospin rotations. Lastly, we apply  $G$ -parity projections, whenever suitable.

The above procedure is applied for two-particle operators having total momenta in the directions of the reference momenta  $\mathbf{p}_{\text{ref}}$  in Table II. An operator having total momentum in any other direction is obtained by applying the appropriate reference rotation  $R_{\text{ref}}$  in Table II to the appropriate operator having momentum in a reference direction.

In order to test the effectiveness of the two-hadron operators that we have designed, we examined the effective

masses associated with the correlators of a variety of two-hadron operators. We also evaluated several correlation matrices mixing single and two-hadron operators. Samples of our results are shown in Figs. 4–6.

In the left plot of Fig. 4, effective masses using  $dt = 3$  associated with a two-meson operator in the  $T_{1u}$  irrep are shown. The two-meson operator has total isospin  $I = \frac{1}{2}$  and zero total momentum and is constructed from single-site kaon and pion operators having equal and opposite on-axis momenta of minimal nonzero magnitude. Results on the  $(24^3|390)$  and  $(32^3|240)$  ensembles are shown and compared to the energies of a free  $\pi$  plus a free  $K$ , indicated by horizontal dashed lines.

An alternative design for a two-hadron operator is to use a suitable localized operator. For example, localized  $\pi\pi$  operators in the  $I = 2, A_{1g}^+$  and  $I = 1, T_{1u}^+$  channels can be obtained using

$$(\pi\pi)^{A_{1g}^+}(t) = \sum_{\mathbf{x}} \pi^+(\mathbf{x}, t) \pi^+(\mathbf{x}, t), \quad (29)$$

$$(\pi\pi)^{T_{1u}^+}(t) = \sum_{\mathbf{x}, k=1,2,3} \{ \pi^+(\mathbf{x}, t) \Delta_k \pi^0(\mathbf{x}, t) - \pi^0(\mathbf{x}, t) \Delta_k \pi^+(\mathbf{x}, t) \}, \quad (30)$$

where  $\pi(\mathbf{x}, t)$  is a single-site pion field using a standard  $\gamma_5$  construction with the LapH-smearred quark fields, and  $\Delta_k \pi(\mathbf{x}, t) = \pi(\mathbf{x} + \hat{\mathbf{k}}, t) - \pi(\mathbf{x} - \hat{\mathbf{k}}, t)$ . The superscripts indicate the electric charges associated with each field. In such localized  $\pi\pi$  operators, the individual pions do not have definite momenta.

The center and right plots of Fig. 4 compare the effective masses for our  $\pi\pi$  operators to those for these localized  $\pi\pi$  operators. The center plot of Fig. 4 shows the  $dt = 3$

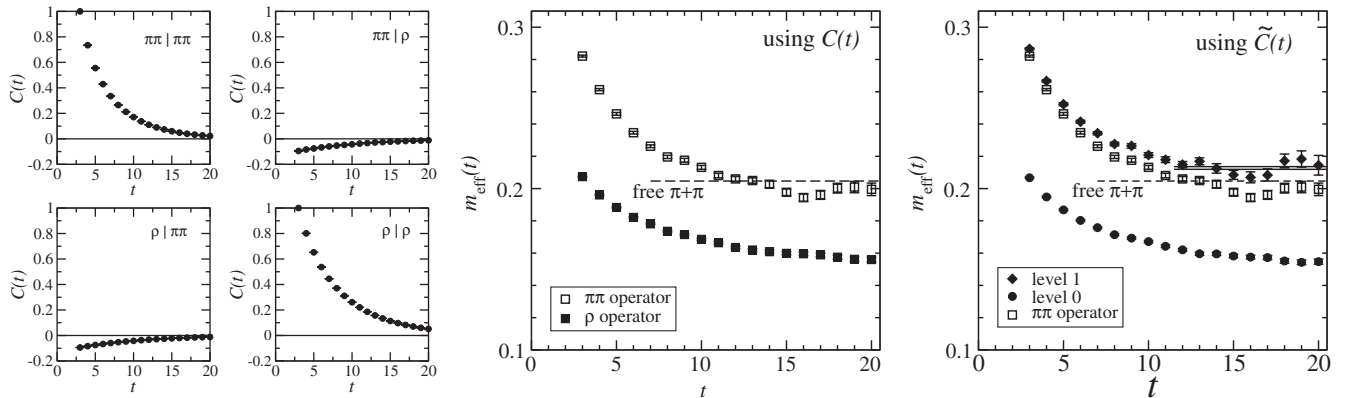


FIG. 5. Mixing of a quark-antiquark single-site  $\rho$  operator and a two-pion operator. Both operators transform according to the  $T_{1u}^+$  irrep and create states of zero total momentum. In the two-pion operator, each pion is a single-site operator traveling with minimal nonzero on-axis momenta. (Left) The  $2 \times 2$  correlation matrix  $C'_{ij}(t) = C_{ij}(t)(C_{ii}(\tau_N)C_{jj}(\tau_N))^{-1/2}$  with  $\tau_N = 3$  in terms of temporal lattice spacing  $a_t$ . (Center) Effective masses,  $m_{\text{eff}}(t)$  using  $dt = 3$ , associated with the diagonal elements of the original correlator matrix  $C(t)$ . (Right) Effective masses associated with the diagonal elements of the rotated correlator  $\tilde{C}(t)$  defined in Eq. (32), compared to the effective mass (hollow squares) of the  $\pi\pi$  operator as also shown in the center plot. The horizontal dashed lines show the location of the free  $\pi + \pi$  energy. The horizontal solid lines show the fit value of the energy of the interacting  $\pi\pi$  state. These results were obtained on the  $(24^3|390)$  ensemble.

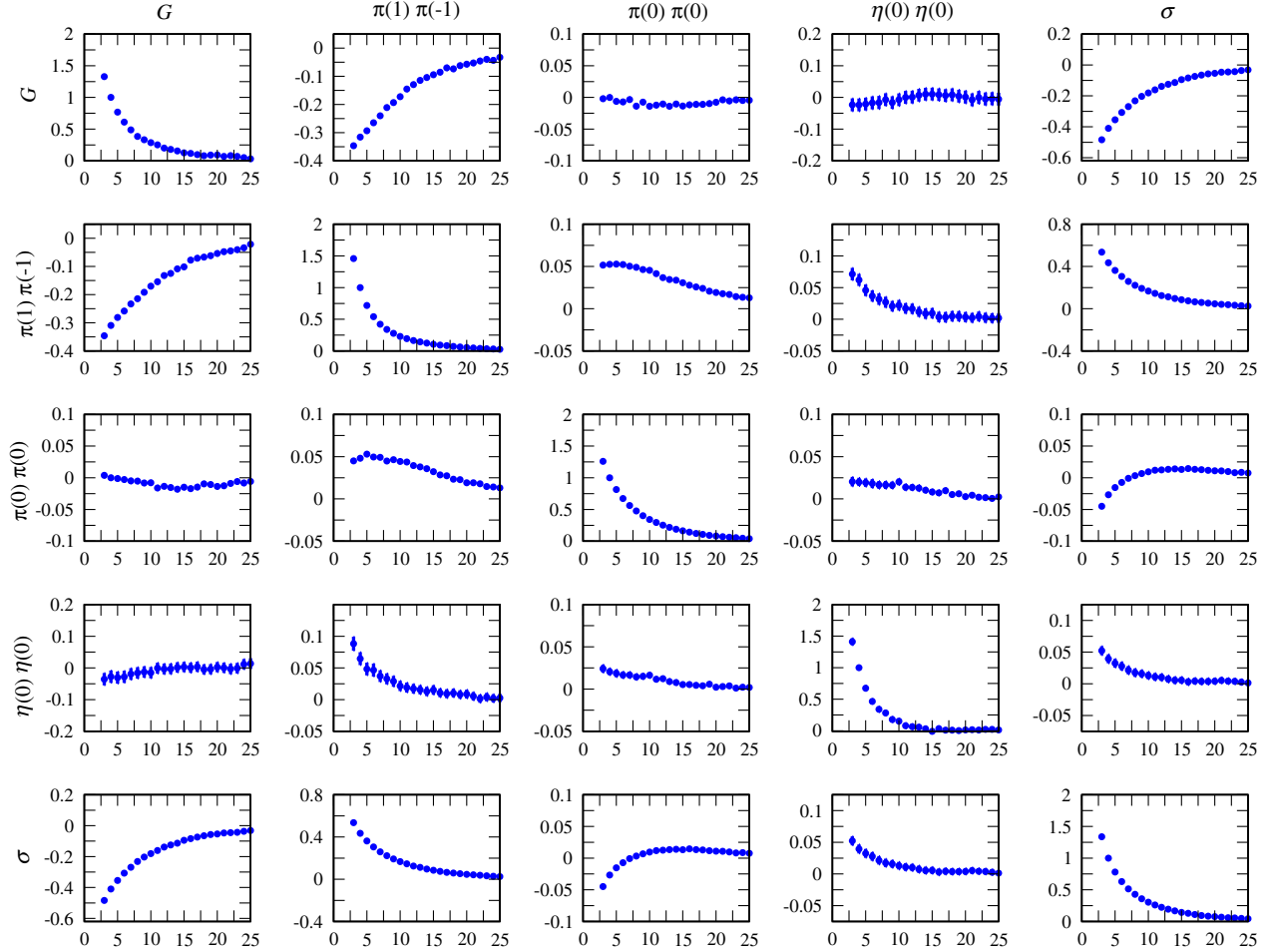


FIG. 6 (color online). The  $5 \times 5$  matrix  $C'_{ij}(t) = C_{ij}(t)(C_{ii}(\tau_N)C_{jj}(\tau_N))^{-1/2}$ , with  $\tau_N = 4$ , of the temporal correlations of five isoscalar operators in the scalar  $A_{1g}^+$  sector for the  $(24^3|390)$  ensemble.  $G$  is the  $G_\Delta$  glueball operator described in Sec. VI, and  $\sigma$  refers to a single-site quark-antiquark operator. Three of the operators are  $I = 0$  two-meson operators constructed out of single-site single-meson operators having equal and opposite momenta. In the  $\eta(0)\eta(0)$  and  $\pi(0)\pi(0)$  operators, each meson has zero momentum, whereas each pion in the  $\pi(1)\pi(-1)$  has minimal nonzero on-axis momentum. Note that large vacuum expectation values have been subtracted to obtain each of these correlators.

effective mass for one of our  $I = 1$   $\pi(1)\pi(-1)$  operators in the  $T_{1u}^+$  channel, consisting of single-site pion operators having equal and opposite on-axis momenta of minimal nonzero magnitude, compared to the effective mass of the localized  $\pi\pi$  operator, given in Eq. (30), on the  $(24^3|390)$  ensemble. The right plot of Fig. 4 shows the effective mass for one of our  $I = 2$   $\pi(0)\pi(0)$  operators in the  $A_{1g}^+$  channel, consisting of single-site pion operators each having zero momenta, compared to the effective mass of the localized  $\pi\pi$  operator, given in Eq. (29), on the  $(24^3|390)$  ensemble. One sees that the effective masses of the localized  $\pi\pi$  operators lie well above those of our operators, indicating that they contain much more excited-state contamination. These effective masses are compared to the energies of the ground state  $\rho$  and the free  $\pi + \pi$  energies, indicated by horizontal dashed lines, in this figure. Note that, in addition to having much less excited-state contamination, the two-pion operators comprised of individual pions having

definite momenta are also much easier to make in large numbers, compared to the localized multihadron operators.

The mixing of a single-site  $\rho$  quark-antiquark operator and a two-pion operator is examined in Fig. 5. Both operators transform according to the  $T_{1u}^+$  irrep and create states of zero total momentum. In the two-pion operator, each pion is a single-site operator traveling with minimal nonzero on-axis momenta. In the left plot, the  $2 \times 2$  real and symmetric correlation matrix  $C'_{ij}(t) = C_{ij}(t) \times (C_{ii}(\tau_N)C_{jj}(\tau_N))^{-1/2}$ , with  $\tau_N = 3$ , is shown. Irrelevant normalization factors are removed by dividing the original correlation matrix by  $(C_{ii}(\tau_N)C_{jj}(\tau_N))^{1/2}$  for some early  $\tau_N$ . The condition number of this matrix  $C'(t)$  at time  $t = 4$  is 1.21, and at  $t = 20$ , the condition number is 3.05. In each matrix element label, the symbol to the right of the vertical bar indicates the source operator and the symbol to the left of the vertical bar denotes the sink operator. These results were obtained on the  $(24^3|390)$  ensemble. This figure



provides further evidence that the stochastic LapH method is well suited to studying systems involving the mixing of single and multihadron operators, and that our smearing parameters and noise dilution schemes were chosen judiciously. One sees that there is a small but noticeably nonzero mixing between these operators.

In the center plot of Fig. 5, the effective masses associated with the diagonal elements of the original correlator matrix  $C(t)$  are displayed. A rotated correlation matrix  $\tilde{C}(t)$  can be defined by first solving for the unitary matrix  $U$  in the eigenvalue equation below:

$$C(\tau_0)^{-1/2}C(\tau_D)C(\tau_0)^{-1/2} = U\tilde{C}(\tau_D)U^\dagger, \quad (31)$$

where  $\tilde{C}(\tau_D)$  is a diagonal matrix and  $C(t)$  is the original Hermitian correlation matrix, then writing

$$\tilde{C}(t) = U^\dagger C(\tau_0)^{-1/2}C(t)C(\tau_0)^{-1/2}U. \quad (32)$$

By construction,  $\tilde{C}(\tau_0)$  is the identity matrix, and  $\tilde{C}(\tau_D)$  is a diagonal matrix. For all other times,  $\tilde{C}(t)$  need not be diagonal. Note that  $\tilde{C}(t)$  is not a principal correlator, such as used in Ref. [32], since the diagonalization is not done for every time. We use  $\tau_0 = 8$  and  $\tau_D = 15$ , and we find that  $\tilde{C}(t)$  remains diagonal, within statistical precision, for all  $t$  exceeding  $\tau_D$ . In the right plot in Fig. 5, the effective masses associated with the diagonal elements of  $\tilde{C}(t)$  are shown, and are labeled by level 0 and level 1.

The purpose of Fig. 5 is to demonstrate the effectiveness of the stochastic LapH method in providing estimates of correlation matrices involving both single and two-hadron operators that are accurate enough to allow reliable diagonalizations and extractions of excited-state energies. Here, it is not our intent to carry out a detailed analysis of this correlation matrix. In future work, we shall include many more operators and attempt to extract the energies of a larger number of low-lying stationary states. For now, we only make a few remarks concerning this correlation matrix.

In the center plot, one sees that the effective mass associated with the original  $\rho$  operator tends to the lowest-lying stationary-state energy in this channel, consistent with expectations. The effective mass associated with the two-pion operator nearly levels off at a higher-lying energy, but it will eventually fall to the lowest-lying  $\rho$  energy, given large enough  $t$ . The coupling of our two-pion operator to the  $\rho$  state is nonzero, but apparently much smaller than its coupling to the lowest-lying two-pion stationary state. The first excited-state energy can be revealed by constructing the rotated correlator  $\tilde{C}(t)$  described above. By ensuring the off-diagonal elements of  $\tilde{C}(t)$  are zero within statistical precision for all  $t > \tau_D$ , the effective masses associated with the diagonal elements of  $\tilde{C}(t)$  tend to the two lowest-lying stationary-state energies in this symmetry channel, as shown in the right plot of Fig. 5. The solid horizontal lines indicate the location of the first excited-state energy (level 1) as determined by a single-exponential fit, with wrap-around,

to  $\tilde{C}_{11}(t)$ . An excellent fit quality is obtained, and the uncertainty in the energy from the fit is indicated by the two parallel lines. This energy is compared to the free two-pion energy, indicated by the dashed horizontal line. The effective mass for the original two-pion operator is also shown in the right plot (hollow squares) for comparison. The diagonalization appears to remove the small coupling to the  $\rho$  stationary state.

The effective mass associated with  $\tilde{C}_{00}(t)$  for level 0 shows a very slight downward drift at large  $t$ . This is due to a temporal wrap-around effect in which our operators create a  $\pi\pi$  state and one  $\pi$  propagates forward in time while the other  $\pi$  propagates backwards in time, producing a small contribution that is essentially constant with respect to time. A fit to this correlator using  $A(e^{-Et} + e^{-E(N_t-t)})$ , which ignores this contribution, for times  $t = 17-25$  produces a poor  $\chi^2/\text{dof} = 2.51$ , whereas a fit including a constant term  $A(e^{-Et} + e^{-E(N_t-t)}) + B$  for  $t = 17-25$  produces a good fit quality  $\chi^2/\text{dof} = 1.03$ , with a fit value for the energy  $E = 0.1638(20)$ .

A last example of the effectiveness of the stochastic LapH method in dealing with mixings between single and two-meson operators is given in Fig. 6, which shows a rescaled  $5 \times 5$  correlation matrix  $C'_{ij}(t) = C_{ij}(t) \times (C_{ii}(\tau_N)C_{jj}(\tau_N))^{-1/2}$ , with  $\tau_N = 4$ , of the temporal correlations of five isoscalar operators in the scalar  $A_{1g}^+$  sector for the  $(24^3|390)$  ensemble. The condition number of  $C'(3)$  is 4.82, of  $C'(8)$  is 18.1, and of  $C'(12)$  is 57.7.  $G$  is the  $G_\Delta$  glueball operator described in Sec. VI, and  $\sigma$  refers to a single-site quark-antiquark operator. Three of the operators are  $I = 0$  two-meson operators constructed out of single-site single-meson operators having equal and opposite momenta. In the  $\eta(0)\eta(0)$  and  $\pi(0)\pi(0)$  operators, each meson has zero momentum, whereas each pion in the  $\pi(1)\pi(-1)$  has minimal nonzero on-axis momentum. In this channel, the correlation matrix elements are defined, for  $N_t \rightarrow \infty$ , by

$$C_{ij}(t) = \langle O_i(t)\bar{O}_j(0) \rangle - \langle O_i \rangle \langle \bar{O}_j \rangle. \quad (33)$$

Large vacuum expectation values have been subtracted to obtain each of these correlators. Let  $O_0, O_1, O_2, O_3, O_4$  denote the glueball operator  $G_\Delta$ , the  $\pi(1)\pi(-1)$ , the  $\pi(0)\pi(0)$ , the  $\eta(0)\eta(0)$ , and the  $\sigma$  operators, respectively. The ratios of the diagonal elements of the correlation matrix at time separation  $t = 3$  over the squares of their respective vacuum expectation values for these five operators are shown below:

$$C_{00}(3)/\langle O_0 \rangle^2 = 0.00001205(29),$$

$$C_{11}(3)/\langle O_1 \rangle^2 = 0.006657(32),$$

$$C_{22}(3)/\langle O_2 \rangle^2 = 0.11396(74),$$

$$C_{33}(3)/\langle O_3 \rangle^2 = 0.155(12),$$

$$C_{44}(3)/\langle O_4 \rangle^2 = 0.002371(12).$$

The smallness of these numbers demonstrates the largeness of the vacuum expectation values for these correlators. This is a notoriously difficult channel to study, but the stochastic LapH method appears to produce results of adequate precision, even for the  $\eta\eta \rightarrow \eta\eta$  correlator, which includes many diagrams involving internal quark loops and other same-time quark lines. Additional operators, such as  $\bar{K}K$  and other  $\pi\pi$ ,  $\eta\eta$ , operators are needed to reliably study the physics here. We certainly plan to investigate this channel in much more detail in the future using a larger number of operators.

Table XXI summarizes the different flavor types of single and two-hadron operators that we plan to include in our first survey of the spectrum of stationary-state energies. We plan to study all bosonic and fermionic flavor sectors involving the  $u$ ,  $d$ ,  $s$  quarks that involve up to two meson and meson-baryon pairs. The particle types to be studied in each flavor sector are listed in this table.  $G$  denotes a glueball operator. In this table,  $\pi$  refers to *any* isovector quark-antiquark meson operator with flavor content such as  $\bar{d}u$  (such as  $a$ ,  $b$ ,  $\pi$ , and  $\rho$  mesons),  $\eta$  refers to any  $\bar{u}u + \bar{d}d$  isoscalar meson operator,  $\phi$  refers to any  $\bar{s}s$  isoscalar meson operator,  $K$  refers to any quark-antiquark

TABLE XXI. The following bosonic and fermionic flavor sectors involving only the  $u$ ,  $d$ ,  $s$  quarks will be studied.  $J$  denotes total spin,  $I$  denotes total isospin, and  $S$  is the total strangeness. The particle contents to be studied in each flavor sector are listed.  $G$  denotes a glueball operator. Here,  $\pi$  refers to *any* isovector quark-antiquark meson operator with flavor content such as  $\bar{d}u$  (such as  $a$ ,  $b$ ,  $\pi$ , and  $\rho$  mesons),  $\eta$  refers to any  $\bar{u}u + \bar{d}d$  isoscalar meson operator,  $\phi$  refers to any  $\bar{s}s$  isoscalar meson operator,  $K$  refers to any quark-antiquark operator having flavor content  $\bar{s}u$  or  $\bar{s}d$  such that its strangeness is  $S = 1$ , and  $\bar{K}$  is any quark-antiquark operator having flavor content  $\bar{u}s$  or  $\bar{d}s$  such that its strangeness is  $S = -1$ .

$(-1)^{2J}$	$I$	$S$	Particle content
1	0	0	$\eta$ , $\phi$ , $G$ , $\eta\eta$ , $\eta\phi$ , $\phi\phi$ , $\pi\pi$ , $\bar{K}K$
1	1	0	$\pi$ , $\pi\pi$ , $\eta\pi$ , $\phi\pi$ , $\bar{K}K$
1	2	0	$\pi\pi$
1	$\frac{1}{2}$	1	$K$ , $K\pi$ , $K\eta$ , $K\phi$
1	$\frac{3}{2}$	1	$K\pi$
1	0	2	$KK$
1	1	2	$KK$
-1	$\frac{1}{2}$	0	$N$ , $N\eta$ , $N\phi$ , $N\pi$ , $\Delta\pi$ , $\Lambda K$ , $\Sigma K$
-1	$\frac{3}{2}$	0	$\Delta$ , $\Delta\eta$ , $\Delta\phi$ , $\Delta\pi$ , $N\pi$ , $\Sigma K$
-1	$\frac{5}{2}$	0	$\Delta\pi$
-1	0	-1	$\Lambda$ , $\Lambda\eta$ , $\Lambda\phi$ , $N\bar{K}$ , $\Sigma\pi$ , $\Xi K$
-1	1	-1	$\Sigma$ , $\Sigma\eta$ , $\Sigma\phi$ , $\Sigma\pi$ , $N\bar{K}$ , $\Delta\bar{K}$ , $\Lambda\pi$ , $\Xi K$
-1	2	-1	$\Delta\bar{K}$ , $\Sigma\pi$
-1	$\frac{1}{2}$	-2	$\Xi$ , $\Lambda\bar{K}$ , $\Xi\eta$ , $\Xi\phi$ , $\Xi\pi$ , $\Sigma\bar{K}$ , $\Omega K$
-1	$\frac{3}{2}$	-2	$\Sigma\bar{K}$ , $\Xi\pi$
-1	0	-3	$\Omega$ , $\Xi\bar{K}$ , $\Omega\eta$ , $\Omega\phi$
-1	1	-3	$\Omega\pi$ , $\Xi\bar{K}$

operator having flavor content  $\bar{s}u$  or  $\bar{s}d$  such that its strangeness is  $S = 1$ , and  $\bar{K}$  is any quark-antiquark operator having flavor content  $\bar{u}s$  or  $\bar{d}s$  such that its strangeness is  $S = -1$ . Our current plans do not include states containing two or more baryons or three or more mesons, although the computational technology can easily accommodate such states.

## VI. A NEW GLUEBALL OPERATOR

Determining stationary-state energies in the interesting scalar isoscalar sector will ultimately involve including a scalar glueball operator. Glueballs are hypothetical particles comprised predominantly of gluons, having no valence quarks. Scalar glueball operators are usually constructed using a sum of gauge-invariant loops of the smeared spatial link variables on a single time slice, which is invariant under translations, rotations, and charge conjugation. However, any purely gluonic quantity with similar symmetry properties could presumably be used. LapH quark-field smearing involves the covariant spatial Laplacian  $\tilde{\Delta}$ . The eigenvalues of the Laplacian are invariant under rotations and gauge transformations, and so, are appropriate for a scalar glueball operator. The lowest-lying eigenvalue was studied, as well as other functions of the eigenvalues. We found that essentially any combination of the low-lying eigenvalues worked equally well for studying the scalar glueball. Two operators in particular that we studied are

$$G_{\Delta}(t) = -\text{Tr}[\Theta(\sigma_s^2 + \tilde{\Delta})\tilde{\Delta}], \quad (34)$$

$$G_W(t) = -\text{Tr}[\Theta(\sigma_s^2 + \tilde{\Delta})\tilde{\Delta} \exp(-W\tilde{\Delta}^2)]. \quad (35)$$

The first operator  $G_{\Delta}$  in Eq. (34), which we call the TrLapH operator, is perhaps the simplest operator that one can construct using the eigenvalues of the covariant Laplacian. In the so-called weighted TrLapH operator  $G_W$  in Eq. (35), we used  $W = 64$  in order that only a handful of the lowest-lying eigenvalues contribute.

The effective masses obtained using  $G_{\Delta}$  and  $G_W$  on the  $24^3 \times 128$  ensemble are shown in Fig. 7. These effective masses are compared to that obtained using a standard glueball operator which is a sum of  $3 \times 3$  loops of the smeared gauge link variables that is rotationally and translationally invariant. One observes very little difference between these effective masses, suggesting these operators are comparable in usefulness for studying the scalar glueball. Similar conclusions were reached using the  $32^3 \times 256$  lattice. Each effective mass eventually tends toward the energy of two pions at rest, demonstrating non-negligible coupling of these operators to  $\pi\pi$  states. Thus, we plan to use the simplest operator  $G_{\Delta}(t)$  in future studies involving the scalar glueball.

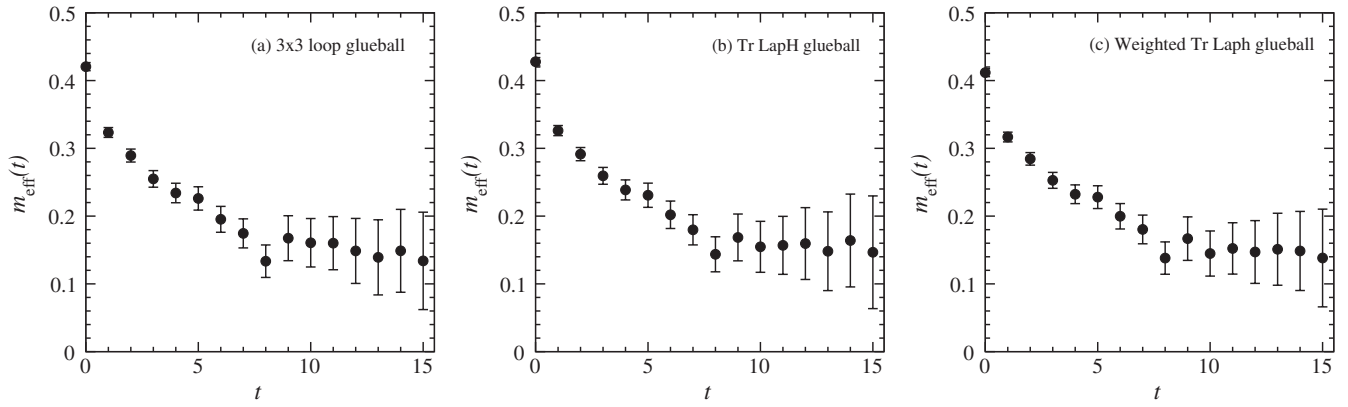


FIG. 7. Comparison of the effective masses,  $m_{\text{eff}}(t)$  using  $dt = 3$ , associated with three different scalar glueball operators on the  $(24^3|390)$  ensemble. (a) The leftmost plot shows the effective mass using an operator defined by a sum of  $3 \times 3$  loops of the smeared gauge link variables that is rotationally and translationally invariant. (b) The middle plot uses the new TrLapH glueball operator  $G_{\Delta}$ , defined in Eq. (34). (c) The rightmost plot shows the results using the weighted TrLapH glueball operator  $G_W$ , defined in Eq. (35). One observes very little difference between these plots, suggesting that these operators are comparable in usefulness for studying the scalar glueball. Each effective mass eventually tends toward the energy of two pions at rest, demonstrating non-negligible coupling of these operators to  $\pi\pi$  states.

## VII. CONCLUSION

Multihadron operators are crucial for reliably extracting the masses of excited states lying above multihadron thresholds in lattice QCD Monte Carlo calculations. Multihadron operators with significant coupling to the low-lying multihadron states of interest can be obtained by combining single-hadron operators of various momenta. The construction and testing of single-hadron operators of definite momentum, and their combinations into two-hadron operators was the main subject of this work.

The approach of Ref. [1] was extended to meson operators of zero momentum, and to both meson and baryon operators having definite nonzero momentum. Our operator design utilizes group-theoretical projections. The point and space groups we use are well known, and the properties of their irreducible representations are widely available in the literature. However, we collected together and presented in this paper some of the specific group theory details needed for our operator construction for the convenience of the reader and to explicitly state our conventions and the notations we use.

Tests of our single-hadron operators using a stochastic method of treating the low-lying modes of quark propagation which exploits Laplacian Heaviside quark-field smearing were presented. These tests were carried out on  $24^3 \times 128$  and  $32^3 \times 256$  anisotropic lattices with pion masses  $m_{\pi} \approx 390$  and  $240$  MeV. A new glueball operator was also introduced and tested. We demonstrated that computing the mixing of this glueball operator with a quark-antiquark operator,  $\pi\pi$ , and  $\eta\eta$  operators is feasible with the stochastic LapH method.

The stochastic LapH method provides reliable estimates of all temporal correlations that will be needed for a

comprehensive survey of the low-lying spectrum of QCD stationary states in finite volume. The method works well even for those correlators that are particularly difficult to compute, such as  $\eta\eta \rightarrow \eta\eta$  in the scalar channel, which involves the subtraction of a large vacuum expectation value. The effectiveness of the method can be traced to two of its key features: the use of noise dilution projectors that interlace in time, and the use of  $Z_N$  noise in the subspace defined by the Laplacian Heaviside quark-field smearing. Introducing noise in the LapH subspace results in greatly reduced variances in temporal correlations compared to methods that introduce noise on the entire lattice. Although the number of Laplacian eigenvectors needed to span the LapH subspace rises dramatically with the spatial volume, the number of inversions of the Dirac matrix needed for a target accuracy is remarkably insensitive to the lattice volume, once a sufficient number of dilution projectors is introduced [6].

In addition to increased efficiency, the stochastic LapH method has other advantages. The method leads to complete factorization of hadron sources and sinks in temporal correlations, which greatly simplifies the logistics of evaluating correlation matrices involving large numbers of operators. Implementing the Wick contractions of the quark lines is also straightforward. Contributions from different Wick orderings within a class of quark-line diagrams differ only by permutations of the noises at the source.

In the future, we plan to carry out a comprehensive survey of the excitation spectrum of the stationary states of QCD involving mesons and baryons containing  $u$ ,  $d$ ,  $s$  quarks. Various scattering phase shifts and decay constants will also be investigated. The needed single-meson and single-baryon sources and sinks for a large number of different momenta have been computed and stored for

three Monte Carlo ensembles. The development and testing of the software to combine these sources and sinks via Wick contractions of the quark fields into temporal correlators has been completed, and the final stages of our operator selections are now in progress. Results for the spectrum, involving both single- and two-hadron operators and using the technology described in this work, will appear in future publications.

### ACKNOWLEDGMENTS

This work was supported by the U.S. National Science Foundation under Grants No. PHY-0510020,

No. PHY-0653315, No. PHY-0704171, No. PHY-0969863, and No. PHY-0970137, and through TeraGrid/XSEDE resources provided by the Pittsburgh Supercomputer Center, the Texas Advanced Computing Center, and the National Institute for Computational Sciences under Grants No. TG-PHY100027 and No. TG-MCA075017. The USQCD QDP ++ library [33] and the Improved BiCGStab solver in Chroma were used in developing the software for the calculations reported here. We acknowledge conversations with Balint Joo, Christian Lang, Daniel Mohler, Mike Peardon, Sasa Prelovsek, and Christopher Thomas.

- 
- [1] S. Basak, R. Edwards, G. Fleming, U. Heller, C. Morningstar, D. Richards, I. Sato, and S. Wallace, *Phys. Rev. D* **72**, 094506 (2005).
- [2] S. Basak, R. Edwards, G. Fleming, U. Heller, C. Morningstar, D. Richards, I. Sato, and S. Wallace, *Phys. Rev. D* **72**, 074501 (2005).
- [3] S. Basak, R. Edwards, G. Fleming, K. Juge, A. Lichtl, C. Morningstar, D. Richards, I. Sato, and S. Wallace, *Phys. Rev. D* **76**, 074504 (2007).
- [4] J. Bulava *et al.*, *Phys. Rev. D* **79**, 034505 (2009).
- [5] C. Morningstar *et al.*, *AIP Conf. Proc.* **1257**, 779 (2010).
- [6] C. Morningstar, J. Bulava, J. Foley, K. Juge, D. Lenkner, M. Peardon, and C. Wong, *Phys. Rev. D* **83**, 114505 (2011).
- [7] J. Foley and C. H. Wong *et al.*, *Proc. Sci.*, LAT2010 (2010) 098 [arXiv:1011.0481].
- [8] J. Bulava and J. Foley *et al.*, *Proc. Sci.*, LAT2010 (2010) 110 [arXiv:1011.5277].
- [9] S. Aoki *et al.*, *Phys. Rev. D* **81**, 074503 (2010).
- [10] M. S. Mahbub, A. O. Cais, W. Kamleh, D. B. Leinweber, and A. G. Williams, *Phys. Rev. D* **82**, 094504 (2010).
- [11] G. P. Engel, C. B. Lang, M. Limmer, D. Mohler, and A. Schafer, *Phys. Rev. D* **82**, 034505 (2010).
- [12] J. Bulava, R. G. Edwards, E. Engelson, B. Joó, H.-W. Lin, C. Morningstar, D. G. Richards, and S. J. Wallace, *Phys. Rev. D* **82**, 014507 (2010).
- [13] J. J. Dudek, R. G. Edwards, B. Joó, M. J. Peardon, D. G. Richards, and C. E. Thomas, *Phys. Rev. D* **83**, 111502 (2011).
- [14] G. P. Engel, C. Lang, M. Limmer, D. Mohler, and A. Schafer, *Phys. Rev. D* **85**, 034508 (2012).
- [15] R. G. Edwards, J. J. Dudek, D. G. Richards, and S. J. Wallace, *Phys. Rev. D* **84**, 074508 (2011).
- [16] M. Mahbub, W. Kamleh, D. B. Leinweber, P. J. Moran, and A. G. Williams, *Phys. Lett. B* **707**, 389 (2012).
- [17] S. Aoki *et al.*, *Phys. Rev. D* **84**, 094505 (2011).
- [18] C. Lang, D. Mohler, S. Prelovsek, and M. Vidmar, *Phys. Rev. D* **84**, 054503 (2011).
- [19] D. Mohler, S. Prelovsek, and R. Woloshyn, *Phys. Rev. D* **87**, 034501 (2013).
- [20] M. S. Mahbub, W. Kamleh, D. B. Leinweber, P. J. Moran, and A. G. Williams, *Phys. Rev. D* **87**, 011501 (2013).
- [21] R. G. Edwards, N. Mathur, D. G. Richards, and S. J. Wallace, *Phys. Rev. D* **87**, 054506 (2013).
- [22] G. Moir, M. Peardon, S. M. Ryan, C. E. Thomas, and L. Liu, *J. High Energy Phys.* **05** (2013) 021.
- [23] C. Alexandrou, T. Korzec, G. Koutsou, and T. Leontiou, arXiv:1302.4410.
- [24] C. E. Thomas, R. G. Edwards, and J. J. Dudek, *Phys. Rev. D* **85**, 014507 (2012).
- [25] C. Morningstar and M. J. Peardon, *Phys. Rev. D* **69**, 054501 (2004).
- [26] M. Peardon, J. Bulava, J. Foley, C. Morningstar, J. Dudek, R. Edwards, B. Joó, H.-W. Lin, D. Richards, and K. Juge, *Phys. Rev. D* **80**, 054506 (2009).
- [27] D. C. Moore and G. T. Fleming, *Phys. Rev. D* **73**, 014504 (2006).
- [28] D. C. Moore and G. T. Fleming, *Phys. Rev. D* **74**, 054504 (2006).
- [29] H.-W. Lin *et al.* (Hadron Spectrum Collaboration), *Phys. Rev. D* **79**, 034502 (2009).
- [30] M. A. Clark, A. D. Kennedy, and Z. Sroczynski, *Nucl. Phys. B, Proc. Suppl.* **140**, 835 (2005).
- [31] J. Foley, K. J. Juge, A. Ó Cais, M. Peardon, S. M. Ryan, and J.-I. Skullerud, *Comput. Phys. Commun.* **172**, 145 (2005).
- [32] B. Blossier, M. Della Morte, G. von Hippel, T. Mendes, and R. Sommer (ALPHA collaboration), *J. High Energy Phys.* **04** (2009) 094.
- [33] R. G. Edwards and B. Joo (SciDAC Collaboration), *Nucl. Phys. B, Proc. Suppl.* **140**, 832 (2005).